

Edge of Chaos Explains Prigogine's Instability of the Homogeneous

Alon Ascoli^{ID}, Senior Member, IEEE, Ahmet S. Demirkol^{ID}, Ronald Tetzlaff, Senior Member, IEEE,
and Leon O. Chua^{ID}, Life Fellow, IEEE

Abstract—One of the complex phenomena, which most attracted the attention of the scientific community over the past few decades, is the emergence of diffusion-driven instabilities in homogeneous cellular media. Explaining this symmetry-breaking process, which the Russian luminary Ilya Prigogine referred to as the Instability of the Homogeneous, is only possible upon invoking the Physics Law of the Edge of Chaos. While the emergence of inhomogeneous static or dynamic periodic solutions in biological reaction-diffusion systems was recently reproduced in two-cell networks, leveraging the Negative Differential Resistance of certain volatile memristors, so far, to the best of our knowledge, no cellular array was ever found to undergo dissipation-induced dynamical phenomena of higher complexity, including a route to chaos, or an uncontrollable upsurge in the respective physical variables. This manuscript determines all the possible sets of conditions on the parameters of a one-port, extracted from the classical Chua circuit, enabling to poised it on some stable and locally-active operating point, employing a deep mathematical analysis, focusing on the properties of its local impedance. The polarisation of the one-port on some Edge of Chaos operating point is the Conditio Sine Qua Non for the Destabilisation of the Homogeneous Solution, resulting in the steady-state appearance of high-order dynamical phenomena, as outlined above, in a simple Reaction-Diffusion Cellular Nonlinear Network, where a linear and passive resistor, interposed between two identical copies of the one-port, lets them interact by means of a diffusion process. Notably, as demonstrated here, whether or not the dissipative coupling path may truly succeed in moving each of the two one-ports of the two-cell array, under study, away from the respective common Edge of Chaos operating point, depends critically upon the satisfaction of the logical disjunction between three inequalities, which enforces the instability of the denominator polynomial of the rational function associated to the local input impedance of the cellular array, as seen across either of the two one-ports.

Index Terms—Local activity, Edge of Chaos, emergent phenomena, diffusion-driven instabilities, turing instability, smale paradox, Chua's circuit, reaction-diffusion cellular nonlinear network.

Manuscript received 24 July 2022; revised 29 October 2022; accepted 7 November 2022. Date of publication 9 November 2022; date of current version 19 December 2022. The work of Leon O. Chua was supported in part by USA AFOSR Grant FA 9550-18-1-0016. This article was recommended by Guest Editor G. C. Sirakoulis. (Corresponding author: Alon Ascoli.)

Alon Ascoli, Ahmet S. Demirkol, and Ronald Tetzlaff are with the Faculty of Electrical and Computer Engineering, Institute of Circuits and Systems, Technische Universität Dresden, 01069 Dresden, Germany (e-mail: alon.ascoli@tu-dresden.de).

Leon O. Chua is with the Department of Electrical Engineering and Computer Sciences, University of California at Berkeley, Berkeley, CA 94720 USA.

Color versions of one or more figures in this article are available at <https://doi.org/10.1109/JETCAS.2022.3221156>.

Digital Object Identifier 10.1109/JETCAS.2022.3221156

I. INTRODUCTION

THE Second Law of Thermodynamics rules out the possibility that emergent phenomena may ever appear in isolated physical media. The Physics Principle of the Edge of Chaos [1], [2], establishing the conditions, under which a non-isolated system may first exhibit complex dynamics, is interpretable as the extension of the Second Law of Thermodynamics to physical media, which may exchange energy with the external environment. In fact, for a system to undergo emergent phenomena, it must be constantly supplied with an ad hoc amount of energy, so as to sit on some bias point, about which it may acquire the capability to amplify infinitesimal fluctuations in energy [3]. This way the system enters an operating regime, known as *Local Activity* [1]. However, for emergent phenomena to appear across its physical medium, the operating point of the locally-active system must additionally be asymptotically stable. Under these circumstances the system is said to be poised on the Edge of Chaos. In such conditions, the system hides a high degree of excitability behind an apparently quiet steady state. Tiny changes to the environmental conditions may then be sufficient to induce the destabilisation of the asymptotically stable operating point of the system, which would then experience some complex dynamical phenomenon, such as limit cycle oscillations, or chaos [4]. To mention an example of complexity *par excellence*, when a biological neuron enters the Edge of Chaos operating regime [5], it is endowed with the capability to generate an All-or-None spike, also known as Action Potential [6], which, enabling synaptic adaptation, underlies the development of intelligence in the brain. Furthermore, through an in-depth analysis of a simple Cellular Neural Network (CNN) [7], leveraging the capability of solid-state volatile threshold switches ([8], [9], [10], [11], [12], [13]) to exhibit, similarly as the sodium and potassium ion channels in a biological neuron [14], a *Negative Differential Resistance* (NDR) [15], which is a signature for Local Activity, it has been recently demonstrated that Edge of Chaos lies behind the emergence of *Turing Instabilities* [16] in reaction-diffusion systems, providing an answer to an open question, which troubled the beautiful mind of the Father of Artificial Intelligence Alan Turing [17]. Last but not least, choosing a bio-inspired circuit, based upon a locally-active memristor from NaM-Lab [18], as the object of the investigations [19], this Physics Principle has also been invoked to resolve the well-known *Smale Paradox* on the wake-up of mathematically-dead cells,

as described in [20], explaining why two identical biological units, sitting on a silent state on their own, may come alive, pulsing together, when allowed to interact by means of a diffusion process, which would be typically expected to equalize the concentrations of corresponding chemical species of the two reaction systems, rather than to induce sustained oscillations [21] across the homogeneous cellular medium. The Russian luminary Ilya Prigogine coined a catchphrase to refer to symmetry-breaking phenomena in homogeneous cellular media, namely the *Instability of the Homogeneous* [22], [23]. So far, to the best of our knowledge, no cellular network has ever been reported to undergo dissipation-induced higher-order dynamics, such as a route to chaos or an uncontrollable upsurge in the respective physical variables [24]. After a brief excursus on the pillars of Local Activity and Edge of Chaos Theory (section II), this paper presents a sixth-order array, in which two identical Chua circuit-based [25], [26] reaction cells, silent on their own, are found to support higher-order complex phenomena of this kind, when let interact by means of a diffusion process, which, in general, would be expected to equalise the cells' dynamical states in pairs. Powerful methods from Nonlinear Dynamics [4] and Local Activity and Edge of Chaos Theory [1] are employed to carry out a comprehensive investigation of the nonlinear dynamics of the Chua circuit (section III-A), so as to identify the conditions necessary and sufficient to poised a reaction cell on the Edge of Chaos (section III-B), which is the *Conditio Sine Qua Non* [16] for the complex phenomenon, referred to by Prigogine as Instability of the Homogeneous, to occur in the two-cell Reaction-Diffusion Cellular Nonlinear Network (RD-CNN) under consideration in this work. Importantly, section III-C derives a triplet of inequalities, whose logical disjunction ensures the dissipation-driven destabilisation of each of the two identical units of this simple RD-CNN away from the common locally-active and stable operating point, featured in the uncoupled case. For some of all the possible circuit parameter regions, which are tabulated in section III-D, and within which the uncoupled cell is poised on the Edge of Chaos, high-order dynamical phenomena may emerge across the proposed RD-CNN, as revealed in the first numerical validation example, presented in section III-E, provided compliance to at least one of the three aforementioned homogeneous solution destabilisation conditions is ensured. Conclusions are finally drawn in section IV. Last but not least, while the body of the manuscript analyses one of the possible schemes to connect the two identical Chua circuits by means of a linear and passive resistor, the appendix summarises the results on our systematic investigation for an alternative coupling arrangement. Remarkably, under the hypothesis of passivity for all the linear components of each of the RD-CNN units, only one (none) of the three possible destabilisation conditions for the homogeneous solution of the two-cell array, may potentially hold true, in the coupling scheme, considered in the body (appendix) of the paper. However, irrespective of the coupling arrangement, for symmetry-breaking effects to induce the development of steady-state chaotic oscillations across the homogeneous cellular medium, at least one of the three two-terminal linear dynamic circuit elements, namely

C_1 , C_2 , and L , sitting in each cell, must necessarily be active.

II. THEORETICAL FOUNDATIONS OF LOCAL ACTIVITY AND EDGE OF CHAOS

Nature obeys Physics Laws. One of them, namely the Edge of Chaos, lies behind the appearance of complexity in non-isolated physical media. The robust foundations of the Local Activity and Edge of Chaos Theory enable to determine under which conditions, on the respective physical parameters, may a medium of this kind support emergent phenomena, which is a crucial preliminary step for design and control applications. This section touches upon those concepts from the Local Activity and Edge of Chaos Theory [1], which will be utilised over the course of the manuscript.

A. II-A. Definitions and Test of Local Activity and Edge of Chaos for One-Ports

Consider a one-port with m -dimensional state \mathbf{x} , scalar input¹ u , and scalar output y . Assume a bias stimulus $u = U$ drives it into some operating point² $\mathbf{Q} = \mathbf{X} = (X_1, \dots, X_m)$, at which the output amounts to Y . Assume that, at some time t_0 , an infinitesimally-small input δu is superimposed on top of the polarisation signal U , resulting in an overall stimulus of the form $u = U + \delta u$. The overall state (output) response of the one-port is then described via $\mathbf{x} = \mathbf{X} + \delta \mathbf{x}$ ($y = Y + \delta y$), where $\delta \mathbf{x}$ (δy) stands for the local signal, which is induced by the infinitesimal input δu , and adds up to the DC component \mathbf{X} (Y). The one-port is said to be Locally Active at \mathbf{Q} if and only if there exists at least one infinitesimally-small perturbation signal δu , such that the local or small-signal net energy $\delta \mathcal{E}|_{\mathbf{Q}}(t_0; t)$, entering the one-port within the time interval $[t_0, t]$, with $t > t_0$, specifically

$$\delta \mathcal{E}|_{\mathbf{Q}}(t_0; t) = \int_{t'=t_0}^{t'=t} \delta u(t') \cdot \delta y(t') dt', \quad (1)$$

becomes negative for at least one finite time instant $t = \bar{t}$ [7]. Equation (1) provides a rigorous definition for the Local Activity of a one-port at a given operating point. However, its adoption to verify whether a one-port, preliminarily polarised at some operating point, may ever enter the Local Activity domain, is practically unfeasible. In fact, before ruling out the possibility that the one-port may ever act as a local source of energy, one should compute the time integral in equation (1) for all t values, under each of the infinitely-many admissible local perturbations, and about any of the generally-uncountable possible operating points of the one-port. Fortunately, however, the *Local Activity Theorem* [1], enunciated below for a m^{th} -order one-port, simplifies this testing investigation.

Remark 1: A m^{th} -order one-port is said to be poised on the Local Activity domain at some operating point \mathbf{Q} if and only if

¹For a current (voltage)-controlled one-port, the input u coincides with the current flowing through (voltage falling across) the one-port, while the output y defines the voltage falling across (the current flowing through) the one-port.

²The components of an operating point \mathbf{Q} of a system with m degrees of freedom are the bias values X_1, \dots, X_m of its m state variables x_1, \dots, x_m . Also, throughout this manuscript, the bias value of a physical variable is highlighted by capitalising the letter, which symbolises the variable itself.

its *small-signal or local transfer function*³ $H|_{\mathbf{Q}}(s)$, evaluated at \mathbf{Q} , satisfies at least one of the following four conditions:

- (i) The i^{th} pole $s = p_i|_{\mathbf{Q}}$ of the local transfer function $H|_{\mathbf{Q}}(s)$ at \mathbf{Q} sits on the right half of the complex plane (RHP), i.e. $\Re\{p_i|_{\mathbf{Q}}\} > 0$ ($i \in \{1, \dots, m\}$).
- (ii) The i^{th} pole $s = p_i|_{\mathbf{Q}}$ of the local transfer function $H|_{\mathbf{Q}}(s)$ at \mathbf{Q} lies on the $j\omega$ axis, i.e. $\Re\{p_i|_{\mathbf{Q}}\} = 0$, and features an either negative real-valued or complex-valued residue $k_{p_i|_{\mathbf{Q}}} = \lim_{s \rightarrow p_i|_{\mathbf{Q}}}(s - p_i|_{\mathbf{Q}}) \cdot H|_{\mathbf{Q}}(s)$ ($i \in \{1, \dots, m\}$).
- (iii) The $i^{\text{th}}, (i+1)^{\text{th}}, \dots$, and $(i+r-1)^{\text{th}}$ poles of the local transfer function $H|_{\mathbf{Q}}(s)$ at \mathbf{Q} , specifically $s = p_i|_{\mathbf{Q}}, s = p_{i+1}|_{\mathbf{Q}}, \dots$, and $s = p_{i+r-1}|_{\mathbf{Q}}$, where $i \in \{1, \dots, m-r+1\}$, and $r \in \{2, \dots, m-i+1\}$, are located on the same position along the $j\omega$ axis.
- (iv) The real part of the local transfer function $H|_{\mathbf{Q}}(s)$, expressed in the Fourier transform domain, i.e. with $s = j\omega$, at \mathbf{Q} , namely $\Re\{H|_{\mathbf{Q}}(j\omega)\}$, is negative for at least one finite real value ω_0 of the angular frequency ω .

While Local Activity is an essential condition for the appearance of emergent phenomena across a physical medium, the epicentre of complexity resides in the Edge of Chaos. In order to operate on the Edge of Chaos a system needs to be both locally active and asymptotically stable at the respective operating point. The *Edge of Chaos Corollary* [1], reported below for a one-port, dictates the rather stringent conditions, enabling a system to enter the Edge of Chaos domain, which is typically referred to as the Pearl of Local Activity, since it holds the seed for complexity [1].

Remark 2: A m^{th} -order one-port is said to be poised on the Edge of Chaos at some operating point \mathbf{Q} if and only if

- (j) Each of the m poles $p_1|_{\mathbf{Q}}, \dots, p_m|_{\mathbf{Q}}$ of its local transfer function $H|_{\mathbf{Q}}(s)$ at \mathbf{Q} lies on the open left half of the complex plane (LHP), implying the operating point asymptotic stability.
- (jj) The sign of the real part of its local transfer function $H|_{\mathbf{Q}}(s)$, evaluated for $s = j\omega$ about \mathbf{Q} , is negative for at least one real-valued angular frequency ω_0 within the range $(-\infty, \infty)$.

The Edge of Chaos test for a m^{th} -order one-port, preliminarily biased at some operating point \mathbf{Q} , requires to verify that none of the four conditions from the Local Activity Theorem, except the one listed in item (iv) from Remark 1, holds true.⁴

B. II-B. Edge of Chaos Theorem

The *Edge of Chaos Theorem* asserts that, for the homogeneous solution of a homogeneous cellular array to lose stability, under the effects of a diffusion process, it is necessary

³For a current-controlled (voltage-controlled) one-port, the local transfer function $H|_{\mathbf{Q}}(s)$ at \mathbf{Q} coincides with the local impedance $Z|_{\mathbf{Q}}(s) \triangleq \frac{\mathcal{L}\{\delta v(t)\}}{\mathcal{L}\{\delta i(t)\}}|_{\mathbf{Q}}$ (local admittance $Y|_{\mathbf{Q}}(s) \triangleq \frac{\mathcal{L}\{\delta i(t)\}}{\mathcal{L}\{\delta v(t)\}}|_{\mathbf{Q}}$) at \mathbf{Q} .

⁴In fact, strictly speaking, for a one-port to be poised on the Edge of Chaos at a given operating point, the denominator of its local transfer function about that operating point is further not allowed to feature a simple root with positive-valued residue on the imaginary axis.

for each of its identical cells to be poised on a locally active and asymptotically stable operating point, when decoupled from all the other ones. The Edge of Chaos Theorem explains the origin for the high-order dynamical phenomena emerging across the homogeneous RD-CNN under the magnifying glass in this manuscript.

III. EDGE OF CHAOS BEHIND THE SILENCE-TO-CHAOS TRANSITION IN A TWO-CELL REACTION-DIFFUSION ARRAY OF CHUA'S CIRCUITS

A. III-A. Cell Circuit, ODE, Operating Point Configurations, and Local Model, toward the Reaction-Diffusion Network Design

Fig. 1(a) shows one of the most studied nonlinear dynamical circuits in the literature, referred to as Chua's circuit [25], [26], where \mathcal{R} denotes a nonlinear and active voltage-controlled resistor with constitutive relationship of the form

$$i_{\mathcal{R}} = g_{\mathcal{R}}(v_{\mathcal{R}}) \triangleq g_1 \cdot v_{\mathcal{R}} + g_3 \cdot v_{\mathcal{R}}^3, \quad (2)$$

in which, by hypothesis,

$$g_1 < 0 \Omega^{-1}, \text{ while } g_3 > 0 \Omega^{-1} \cdot V^{-2}. \quad (3)$$

Defining three state variables as the voltage v_{C_1} across capacitor C_1 , the voltage v_{C_2} across capacitor C_2 , and the current i_L through inductor⁵ L , applying Kirchhoff's Voltage and Current Laws [28] to the Chua circuit from Fig. 1(a) enables to cast its mathematical model in the following form:

$$\frac{dv_{C_1}}{dt} = \frac{1}{C_1} \cdot \left(\frac{v_{C_2} - v_{C_1}}{R} - i_{\mathcal{R}}(v_{C_1}) \right), \quad (4)$$

$$\frac{dv_{C_2}}{dt} = \frac{1}{C_2} \cdot \left(i_L - \frac{v_{C_2} - v_{C_1}}{R} \right), \text{ and} \quad (5)$$

$$\frac{di_L}{dt} = \frac{1}{L} \cdot (-R_0 \cdot i_L - v_{C_2}), \quad (6)$$

where R and R_0 denote two linear resistors.

Let us now consider two identical circuits, of the kind shown in Fig. 1(a), calling them cells 1 and 2 (see Fig. 2).

In the discussion to follow, the three state variables and the Chua diode voltage and current for the cell j , with $j \in \{1, 2\}$, are referred to as $v_{C_{1,j}}$, $v_{C_{2,j}}$, $i_{L,j}$, $v_{\mathcal{R},j}$, and $i_{\mathcal{R},j}$, respectively. Let us now couple diffusively these two reaction cells through the corresponding ports A_1-B_1 and A_2-B_2 . Specifically, a linear and passive resistor of resistance R_C is inserted between terminals A_1 and A_2 , while terminals B_1 and B_2 are shorted one with the other. The two-cell reaction-diffusion network may be mathematically modelled by the following sixth-order ODE system:

$$\begin{aligned} \frac{dv_{C_{1,1}}}{dt} &= \frac{1}{C_1} \\ &\cdot \left(\frac{v_{C_{2,1}} - v_{C_{1,1}}}{R} - i_{\mathcal{R},1}(v_{C_{1,1}}) - \frac{v_{C_{1,1}} - v_{C_{1,2}}}{R_C} \right), \end{aligned} \quad (7)$$

⁵Very interestingly, a novel inductorless hardware implementation of the Chua circuit, employing only two active components, has been just proposed in [27].

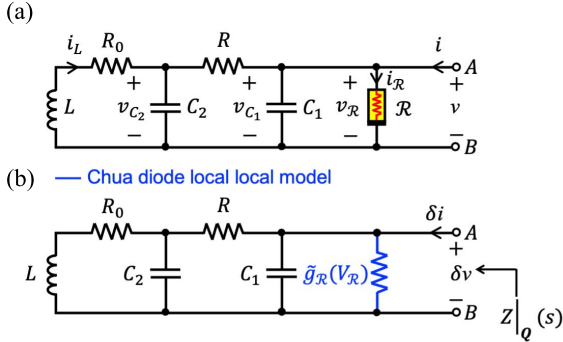


Fig. 1. (a) The Chua circuit. Here i and v denote port current and voltage of a one-port with access terminals A and B . The port $A-B$ will be employed shortly to couple two identical copies of this circuit through a linear and passive resistor of resistance R_C . (b) Small-signal equivalent circuit model of the aforementioned one-port about a given operating point $\mathbf{Q} = (V_{C_1}, V_{C_2}, I_L)$ (note that the bias level I of the current i at port $A-B$ is identically null). Here $\tilde{g}_R = \tilde{g}_R(V_R)$, in which $V_R \equiv V_{C_1}$, denotes the small-signal conductance of the Chua diode \mathcal{R} about the first component of the one-port operating point \mathbf{Q} . This linear circuit may be employed to determine the infinitesimal voltage signal δv , which adds up to the bias level $V \equiv V_{C_1}$, as it falls across the aforementioned one-port in response to any local current stimulus δi , which slightly perturbs the one-port itself away from \mathbf{Q} . $Z|_{\mathbf{Q}}(s)$ is the local impedance of the Chua circuit, as seen from the port $A-B$.

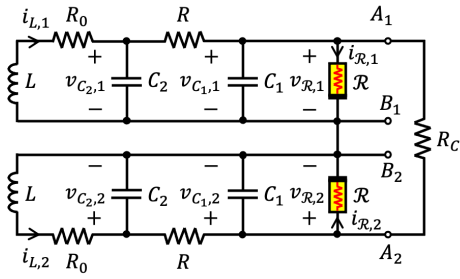


Fig. 2. Array of two identical diffusively-coupled Chua circuit-based reaction cells. Ports A_1-B_1 and A_2-B_2 are employed to establish a physical connection between the two cells. Particularly, a linear and passive resistor of resistance R_C is interposed between nodes A_1 and A_2 , while nodes B_1 and B_2 are joined together.

$$\frac{dv_{C_{2,1}}}{dt} = \frac{1}{C_2} \cdot \left(i_{L,1} - \frac{v_{C_{2,1}} - v_{C_{1,1}}}{R} \right), \quad (8)$$

$$\frac{di_{L,1}}{dt} = \frac{1}{L} \cdot (-R_0 \cdot i_{L,1} - v_{C_{2,1}}), \quad (9)$$

$$\begin{aligned} \frac{dv_{C_{1,2}}}{dt} &= \frac{1}{C_1} \\ &\cdot \left(\frac{v_{C_{2,2}} - v_{C_{1,2}}}{R} - i_{\mathcal{R},2}(v_{C_{1,2}}) + \frac{v_{C_{1,1}} - v_{C_{1,2}}}{R_C} \right), \end{aligned} \quad (10)$$

$$\frac{dv_{C_{2,2}}}{dt} = \frac{1}{C_2} \cdot \left(i_{L,2} - \frac{v_{C_{2,2}} - v_{C_{1,2}}}{R} \right), \text{ and} \quad (11)$$

$$\frac{di_{L,2}}{dt} = \frac{1}{L} \cdot (-R_0 \cdot i_{L,2} - v_{C_{2,2}}), \quad (12)$$

For simplicity, in the remainder of this paper, we let

$$R_0 = 0 \Omega. \quad (13)$$

The objective of the analysis to follow is to identify all the possible regions of the parameter space, where either of the two identical cells of the array from Fig. 2, when decoupled

from the other cell, is poised on the Edge of Chaos about a given operating point⁶ \mathbf{Q} . As follows from the Edge of Chaos Theorem from section II-A, this is the *Conditio Sine Qua Non* for the counterintuitive destabilisation of the common operating point of the two uncoupled cells, as a diffusion process activates their interaction.

Let us commence the investigations by determining all the admissible operating points for the basic reaction cell of Fig. 1(a). A possible operating point \mathbf{Q} for the third-order Chua circuit is an admissible equilibrium point (V_{C_1}, V_{C_2}, I_L) for the set of three coupled nonlinear ODEs (4)–(6). Under the assumption (13), this third-order autonomous ODE system may admit:

- 1) three equilibria, namely

$$\mathbf{Q}_0 \triangleq (V_{C_{1,0}}, V_{C_{2,0}}, I_{L,0}) = (0, 0, 0), \quad (14)$$

$$\begin{aligned} \mathbf{Q}_{-} &\triangleq (V_{C_{1,-}}, V_{C_{2,-}}, I_{L,-}) \\ &= \left(-\sqrt{\frac{-(1 + g_1 \cdot R)}{g_3 \cdot R}}, 0, \frac{1}{R} \cdot \sqrt{\frac{-(1 + g_1 \cdot R)}{g_3 \cdot R}} \right), \end{aligned}$$

and

$$(15)$$

$$\mathbf{Q}_{+} \triangleq (V_{C_{1,+}}, V_{C_{2,+}}, I_{L,+}) = -\mathbf{Q}_{-}, \quad (16)$$

if

$$R > 0, \text{ and } 1 + g_1 \cdot R < 0, \text{ or if} \quad (17)$$

$$R < 0; \quad (18)$$

- 2) one equilibrium only, namely \mathbf{Q}_0 from equation (14), if

$$R > 0, \text{ and } 1 + g_1 \cdot R > 0. \quad (19)$$

All in all, the number of possible operating points for the Chua circuit depends upon two of its parameters, specifically g_1 , and R . In fact, conditions (17), (18), and (19) identify three main case studies, which are respectively referred to as A, B, and C, in the discussion to follow. Throughout the study, presented in this manuscript, g_1 , and g_3 are in turn fixed to -0.75 mS, and $37.6 \mu \text{S} \cdot \text{V}^{-2}$. Figs. 3(a), or 3(b), 4, and 5, associated to a possible scenario in case study A, B, and C, respectively,⁷ illustrate in turn the intersections of the current $i_{\mathcal{R}}$ -voltage $v_{\mathcal{R}}$ characteristic of the nonlinear resistor \mathcal{R} (solid blue trace) with the load line $i_{\mathcal{R}} = -v_{\mathcal{R}}/R$ for the Chua diode (dashed black trace), as extracted from the reaction cell of Fig. 1(a) under DC operating conditions, when the first, second, and third value

⁶Obviously, with reference to Fig. 1(a), any operating point \mathbf{Q} for the one-port with access terminals A and B also defines an admissible operating point for the Chua circuit, from which the one-port is extracted.

⁷In anticipation for the analysis reported below, it may be important to mention, already at this point, that Figs. 3, 4, and 5 also depict the possible operating point stability configurations for the Chua circuit in case studies A, B, and C, respectively. A filled/hollow circle marker is employed to mark a DC diode voltage-current pair $P = (V_{\mathcal{R}}, I_{\mathcal{R}})$, featuring ordinate $I_{\mathcal{R}} = g_{\mathcal{R}}(V_{\mathcal{R}})$, and abscissa $V_{\mathcal{R}} = V_{C_1}$, and associated to a stable/unstable cell operating point $\mathbf{Q} = (V_{C_1}, V_{C_2}, I_L)$. As inferable from Fig. 3, in case study A, two operating point stability configurations are possible for the ODE system (4)–(6), one, where the Chua circuit is stable both at \mathbf{Q}_{-} , and at \mathbf{Q}_{+} (refer to the scenario, illustrated in plot (a)), and one, with \mathbf{Q}_0 GAS (refer to the scenario, illustrated in plot (b)).

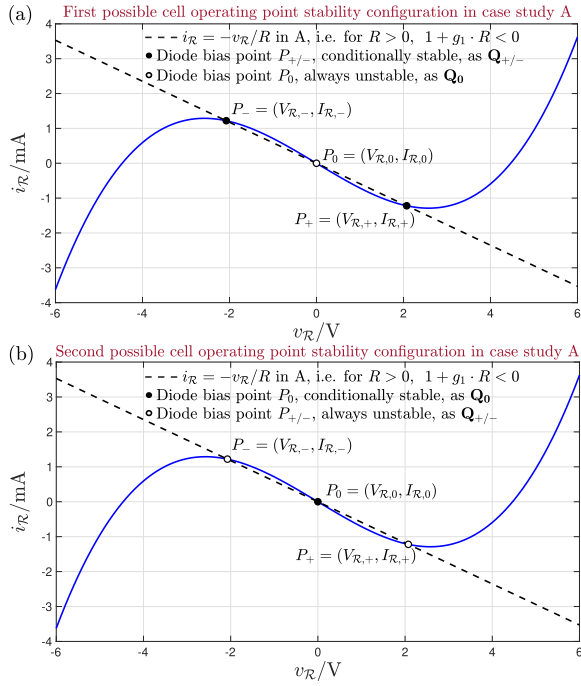


Fig. 3. Demonstration for the existence of two admissible operating point stability configurations for the one-port with access terminals A and B from Fig. 1(a) in case study A, i.e. under the hypothesis established by equation (17), and the assumptions (3) and (13). The solid blue trace in either of the two plots illustrates the current i_R -voltage v_R characteristic of the Chua diode \mathcal{R} for $g_1 = -0.75 \text{ mS}$, and $g_3 = 37.6 \mu\text{S} \cdot \text{V}^{-2}$. The dashed black trace, appearing in both plots (a) and (b), depicts the load line $i_R = -v_R/R$ for the Chua diode, as extracted for the reaction cell of Fig. 1(a) under DC operating conditions, when $1.7 \text{ k}\Omega$ is assigned to the resistance of the resistor R . The three circle markers in either of the two plots indicate the triplet of admissible Chua diode bias points, specifically $P_- = (V_{R,-}, I_{R,-})$, $P_0 = (V_{R,0}, I_{R,0})$, and $P_+ = (V_{R,+}, I_{R,+})$ in this representative example of interest from case study A. P_0 ($P_{-/+}$), featuring ordinate $I_{R,0} = g_{\mathcal{R}}(V_{R,0})$ ($I_{R,-/+} = g_{\mathcal{R}}(V_{R,-/+})$), and abscissa $V_{R,0} = V_{C_1,0}$ ($V_{R,-/+} = V_{C_1,-/+}$), corresponds to the operating point \mathbf{Q}_0 ($\mathbf{Q}_{-/+}$) for the two-terminal circuit element with port A-B from Fig. 1(a). With reference to plot (a) (b), under suitable conditions, as reported in either row A.1.A, or A.1.B, or even A.2.A (in row A.2.B) from Table I, \mathbf{Q}_0 is (\mathbf{Q}_- and \mathbf{Q}_+ are) unstable, whereas the aforementioned one-port is poised on the Edge of Chaos at either \mathbf{Q}_- or \mathbf{Q}_+ (at \mathbf{Q}_0). Here, and throughout the remainder of this paper, the instability/stability of an operating point \mathbf{Q} of the one-port under test is indicated by the hollow/filled nature of the circle, indicating the location of the associated Chua diode bias point P .

from the set $\{1.7, -8.5, 1\} \text{ k}\Omega$ is assigned⁸ to the resistance R . Assuming the Chua circuit to sit in a certain operating point \mathbf{Q} , the local model of the respective Chua diode, featuring a bias voltage $V_{\mathcal{R}} \equiv V_{C_1}$, may be cast as

$$\delta i_{\mathcal{R}} = \tilde{g}_{\mathcal{R}}(V_{C_1}) \cdot \delta v_{\mathcal{R}}, \quad (20)$$

where

$$\tilde{g}_{\mathcal{R}}(V_{C_1}) = g_1 + 3 \cdot g_3 \cdot V_{C_1}^2, \quad (21)$$

is the diode local conductance at the respective bias point,⁹ i.e.

$$\tilde{g}_{\mathcal{R}}(V_{C_1}) = \begin{cases} g_1, & \text{about } P_0, \text{ or} \\ -2 \cdot g_1 - \frac{3}{R}, & \text{about either } P_- \text{ or } P_+ \end{cases} \quad (22a)$$

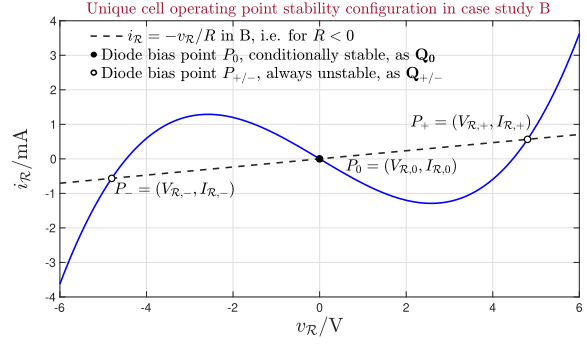


Fig. 4. Exemplary scenario of interest from case study B, i.e. under the constraint set by equation (18), and the assumptions (3) and (13), demonstrating how, here, the two-terminal element with port A-B from Fig. 1(a) may admit one and only one possible operating point stability configuration. While the solid blue trace represents the graph of the Chua diode constitutive relationship from equation (2) under the parameter setting reported in the caption of Fig. 3, the dashed black line is the $i_R = -v_R/R$ versus v_R locus for $R = -8.5 \text{ k}\Omega$. Provided each of the inequalities, listed along row B.1 from Table I, applies, the one-port under consideration is locally active but unstable (is polarised in the Edge of Chaos domain) at either of the off-the-origin operating points \mathbf{Q}_- and \mathbf{Q}_+ (at the operating point \mathbf{Q}_0 in the origin of the $v_{C_1}-v_{C_2}-i_L$ state space), which respectively correspond to the diode bias points P_- and P_+ (which corresponds to the diode bias point P_0). The caption of Fig. 3 reports details on the coordinates of the three admissible diode bias points in case study B.

With reference to Fig. 1(a), no current flows into node A under DC conditions, when, as a result, $i = I = 0 \text{ A}$. Superimposing on this DC level an infinitesimal stimulus δi , the total current, entering node A, becomes $i = I + \delta i = \delta i$. Let δv indicate the small-signal voltage response of the one-port with access terminals A and B from this figure to the infinitesimal stimulus δi . The total voltage, falling across the one-port, may then be expressed as $v = V + \delta v$, where $V \equiv V_{C_1}$. Linearising the ODE set (4)-(6) about a given operating point $\mathbf{Q} = (V_{C_1}, V_{C_2}, i_L)$, and transforming the resulting equations in the Laplace domain, the small-signal impedance $Z|_{\mathbf{Q}}(s)$ of the Chua circuit of Fig. 1(a), as seen from the port A-B, about \mathbf{Q} , is found to read as

$$Z|_{\mathbf{Q}}(s) = \left. \frac{\mathcal{L}\{\delta v(t)\}}{\mathcal{L}\{\delta i(t)\}} \right|_{\mathbf{Q}} = \frac{N|_{\mathbf{Q}}(s)}{D|_{\mathbf{Q}}(s)} = \frac{K \cdot (s^2 + a_1 \cdot s + a_0)}{s^3 + b_2|_{\mathbf{Q}} \cdot s^2 + b_1|_{\mathbf{Q}} \cdot s + b_0|_{\mathbf{Q}}}, \quad (23)$$

from which it is straightforward to infer the formulas for the numerator and denominator polynomials, indicated as $N|_{\mathbf{Q}}(s)$ and $D|_{\mathbf{Q}}(s)$, respectively, while

$$K \triangleq \frac{1}{C_1}, \quad (24)$$

$$a_1 \triangleq \frac{1}{R \cdot C_2}, \quad (25)$$

$$a_0 \triangleq \frac{1}{L \cdot C_2}, \quad (26)$$

$$b_2|_{\mathbf{Q}} \triangleq \frac{C_1 + C_2 \cdot (1 + R \cdot \tilde{g}_{\mathcal{R}}(V_{C_1}))}{R \cdot C_1 \cdot C_2}, \quad (27)$$

⁸With reference to Figs. 3 and 4, $\mathbf{P}_{-/+}$ ($\mathbf{Q}_{-/+}$) indicate either of the two diode (cell) off-the-origin operating points.

⁹The diode bias point P_0 ($P_{-/+}$) is unequivocally associated to the cell operating point \mathbf{Q}_0 ($\mathbf{Q}_{-/+}$).

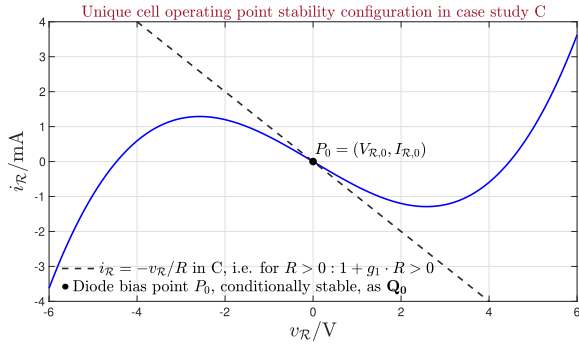


Fig. 5. Proof of evidence for the uniqueness of the operating point stability configuration for the one-port, featuring access terminals A and B , and extracted from the Chua circuit of Fig. 1(a), in case study C, i.e. under the condition, dictated by equation (19), and the assumptions (3) and (13). The solid blue trace shows the Chua diode characteristic (the values assigned to g_1 and g_3 are provided in the caption of Fig. 3). The dashed black trace visualises the $i_R = -v_R/R$ versus v_R locus for $R = 1 \text{ k}\Omega$. The circle marker stands for the only possible Chua diode bias point, specifically P_0 , in this illustrative example of interest from case study C (P_0 is unequivocally associated to the operating point \mathbf{Q}_0 of the aforementioned one-port, as described in the caption of Fig. 3). Under particular constraints on its parameters, as reported in either row C.1.A or C.1.B, or even C.2 from Table I, the one-port under test operates in the Edge of Chaos regime at \mathbf{Q}_0 .

$$b_1|_{\mathbf{Q}} \triangleq \frac{\tilde{g}_{\mathcal{R}}(V_{C_1}) \cdot L + C_1 \cdot R}{C_1 \cdot C_2 \cdot L \cdot R}, \text{ and} \quad (28)$$

$$b_0|_{\mathbf{Q}} \triangleq \frac{1 + \tilde{g}_{\mathcal{R}}(V_{C_1}) \cdot R}{L \cdot C_1 \cdot C_2 \cdot R}. \quad (29)$$

As may be inferred by inspecting equations (27), (28), and (29), the formulas for the three variable coefficients in the denominator of the rational polynomial function, defining $Z|_{\mathbf{Q}}(s)$ – see equation (23) – depend upon¹⁰ the cell operating point \mathbf{Q} through the respective diode bias point $P = (V_{C_1}, g_{\mathcal{R}}(V_{C_1}))$. Looking at Fig. 1 once more, $Z|_{\mathbf{Q}}(s)$ may be alternatively obtained by applying basic circuit-theoretic principles in the Laplace domain to the one-port local circuit model, depicted in plot (b), and derived from the circuit topology in (a) through the replacement of the only nonlinear two-terminal circuit element in the Chua circuit – namely the diode – with a linear conductor of conductance $g_{\mathcal{R}}(V_{C_1})$ expressed by equation (22a), if $V_{C_1} = V_{C_1,0}$, or by equation (22a), if V_{C_1} is equal to either the first or the second element from the set $\{V_{C_1,-}, V_{C_1,+}\}$. The real part of the local impedance $Z|_{\mathbf{Q}}(s)$ of the one-port with access terminals A and B from Fig. 1(a), for $s = j\omega$, and about a given operating point \mathbf{Q} , is found to be expressed by

$$\Re\{Z|_{\mathbf{Q}}(j\omega)\} = \frac{c_4|_{\mathbf{Q}} \cdot \omega^4 + c_2|_{\mathbf{Q}} \cdot \omega^2 + c_0|_{\mathbf{Q}}}{\omega^6 + d_4|_{\mathbf{Q}} \cdot \omega^4 + d_2|_{\mathbf{Q}} \cdot \omega^2 + d_0}, \quad (30)$$

$$c_4|_{\mathbf{Q}} \triangleq K \cdot (b_2|_{\mathbf{Q}} - a_1), \quad (31)$$

$$c_2|_{\mathbf{Q}} \triangleq K \cdot (a_1 \cdot b_1|_{\mathbf{Q}} - a_0 \cdot b_2|_{\mathbf{Q}} - b_0|_{\mathbf{Q}}), \quad (32)$$

$$c_0|_{\mathbf{Q}} \triangleq K \cdot a_0 \cdot b_0|_{\mathbf{Q}}, \quad (33)$$

$$d_4|_{\mathbf{Q}} \triangleq (b_2|_{\mathbf{Q}})^2 - 2 \cdot b_1|_{\mathbf{Q}}, \quad (34)$$

$$d_2|_{\mathbf{Q}} \triangleq (b_1|_{\mathbf{Q}})^2 - 2 \cdot b_0|_{\mathbf{Q}} \cdot b_2|_{\mathbf{Q}}, \quad (35)$$

¹⁰Given that, according to equation (22a), $g_{\mathcal{R}}(V_{C_1})$ assumes the same expression at $P = P_-$, and at $P = P_+$, since $|V_{C_1,-}| = |V_{C_1,+}|$, testing the cell for Local Activity at each of the off-the-origin operating points $\mathbf{Q} = \mathbf{Q}_-$ and $\mathbf{Q} = \mathbf{Q}_+$ leads to the same conclusions.

$$d_0|_{\mathbf{Q}} \triangleq (b_0|_{\mathbf{Q}})^2. \quad (36)$$

Mathematical calculations reveal that $\Re\{Z|_{\mathbf{Q}}(j\omega)\}$ may admit at most four real-valued zeros at the angular frequencies

$$\omega_{1,2,3,4}|_{\Re\{Z|_{\mathbf{Q}}(j\omega)\}=0} = \mp\sqrt{\eta_{\mp}|_{\mathbf{Q}}}, \quad (37)$$

where

$$\eta_{\mp}|_{\mathbf{Q}} \triangleq \frac{-c_2|_{\mathbf{Q}} \mp \sqrt{\Delta|_{\mathbf{Q}}}}{2 \cdot c_4|_{\mathbf{Q}}}, \quad (38)$$

with

$$\Delta|_{\mathbf{Q}} \triangleq (c_2|_{\mathbf{Q}})^2 - 4 \cdot c_4|_{\mathbf{Q}} \cdot c_0|_{\mathbf{Q}}. \quad (39)$$

Simple mathematical manipulations reveal that $\Re\{Z|_{\mathbf{Q}}(j\omega)\}$ has at least one real-valued zero, on condition that $\Delta|_{\mathbf{Q}} \in \mathbb{R}_{\geq 0}$, which endows the variables from equation (38) with real-valuedness, and, concurrently, at least one between $\eta_-|_{\mathbf{Q}}$ and $\eta_+|_{\mathbf{Q}}$ is non-negative.¹¹

B. III-B. Conditions for Poising the Chua Circuit-based Reaction Cell on the Edge of Chaos

Now, recalling the discussion in section II-A, in order to bias the one-port under study at a locally-active and stable operating point \mathbf{Q} , none of the conditions from the Local Activity Theorem may apply, except for condition (iv). Equivalently, the satisfaction of both conditions (j) and (jj) from the Edge of Chaos Corollary – consult the same section – is necessarily required. In order for the three poles of $Z|_{\mathbf{Q}}(s)$ to lie on the LHP, the following constraints need to be enforced on the variable parameters in the denominator of the rational polynomial function from equation (23), as follows from the Routh-Hurwitz stability criterion [29]: $b_2|_{\mathbf{Q}} > 0$, $b_0|_{\mathbf{Q}} > 0$, and $b_1|_{\mathbf{Q}} \cdot b_2|_{\mathbf{Q}} > b_0|_{\mathbf{Q}}$. Employing equations (27), (28), and (29), the first, second, and third condition in this triplet may be cast as

$$\frac{C_1 + C_2 \cdot (1 + R \cdot \tilde{g}_{\mathcal{R}}(V_{C_1}))}{R \cdot C_1 \cdot C_2} > 0, \quad (40)$$

$$\frac{1 + \tilde{g}_{\mathcal{R}}(V_{C_1}) \cdot R}{L \cdot C_1 \cdot C_2 \cdot R} > 0, \text{ and} \quad (41)$$

$$\frac{\tilde{g}_{\mathcal{R}}(V_{C_1}) \cdot L \cdot (C_1 + C_2 \cdot (1 + \tilde{g}_{\mathcal{R}}(V_{C_1}) \cdot R)) + R \cdot C_1^2}{L} > 0. \quad (42)$$

Note that the constraints $b_2|_{\mathbf{Q}} > 0$, $b_0|_{\mathbf{Q}} > 0$, and $b_1|_{\mathbf{Q}} \cdot b_2|_{\mathbf{Q}} > b_0|_{\mathbf{Q}}$ imply a positive polarity for¹² $b_1|_{\mathbf{Q}}$, i.e., if \mathbf{Q} is asymptotically stable, the following inequality also applies:

$$\frac{\tilde{g}_{\mathcal{R}}(V_{C_1}) \cdot L + C_1 \cdot R}{C_1 \cdot C_2 \cdot L \cdot R} > 0. \quad (43)$$

The satisfaction of condition (iv) from the Local Activity Theorem, reviewed in section II-A, further requires that

¹¹Necessarily, the existence of a zero for $\Re\{Z|_{\mathbf{Q}}(j\omega)\}$ forbids the radicand on the right hand side of equation (37) from holding a negative sign.

¹²For the analysis of some scenario from the case studies, classified in section III-A, the early-on imposition of the redundant condition (43) simplifies the application of the proposed systematic procedure for testing $Z|_{\mathbf{Q}}(s)$ for Edge of Chaos.

the fourth-order polynomial in ω , forming the numerator of $\Re\{Z|_{\mathbf{Q}}(j\omega)\}$ in equation (30), goes negative for some finite real-valued angular frequency ω_0 . This is always the case if $c_4|_{\mathbf{Q}}$ from equation (31) is strictly negative, while, on the proviso that this coefficient holds a positive sign, which calls for the satisfaction of the constraint

$$\frac{1 + \tilde{g}_{\mathcal{R}}(V_{C_1}) \cdot R}{R} > 0, \quad (44)$$

it is necessary firstly that the variables $\eta_{\mp}|_{\mathbf{Q}}$, reported in equation (38), are distinct and real, which enforces a positive sign on $\Delta|_{\mathbf{Q}}$ from equation (39), requiring the inequality

$$1 - \frac{4 \cdot C_2 \cdot R \cdot (1 + \tilde{g}_{\mathcal{R}}(V_{C_1}) \cdot R)}{\tilde{g}_{\mathcal{R}}(V_{C_1}) \cdot L} > 0, \quad (45)$$

to hold true, and, secondly, that $\eta_-|_{\mathbf{Q}}$ and $\eta_+|_{\mathbf{Q}}$ either feature opposite polarities, which implies $\eta_1|_{\mathbf{Q}} \cdot \eta_2|_{\mathbf{Q}} < 0$, expandable as $L^2 \cdot C_2^2 < 0$, and thus, obviously, never true here, or admit a sum, i.e. $\eta_1|_{\mathbf{Q}} + \eta_2|_{\mathbf{Q}}$, of positive polarity, which results in the condition

$$\frac{2 \cdot C_2 \cdot R \cdot (1 + \tilde{g}_{\mathcal{R}}(V_{C_1}) \cdot R) - \tilde{g}_{\mathcal{R}}(V_{C_1}) \cdot L}{L \cdot R \cdot (1 + \tilde{g}_{\mathcal{R}}(V_{C_1}) \cdot R)} > 0. \quad (46)$$

Remark 3: Assume the local transfer function $H|_{\mathbf{Q}}(s)$ of a one-port, about one of its admissible operating points, say \mathbf{Q} , to be expressed by a rational function of the form

$$H|_{\mathbf{Q}}(s) = K|_{\mathbf{Q}} \cdot \prod_{j=1}^n (s - z_j|_{\mathbf{Q}}) / \prod_{i=1}^m (s - p_i|_{\mathbf{Q}}), \quad (47)$$

where $K|_{\mathbf{Q}}$ is a real constant, $z_j|_{\mathbf{Q}}$ ($p_i|_{\mathbf{Q}}$) denotes its j^{th} (i^{th}) zero (pole), and $n \leq m$. When constraints are enforced on the one-port parameters, so that all the m poles $p_1|_{\mathbf{Q}}, \dots, p_m|_{\mathbf{Q}}$ of $H|_{\mathbf{Q}}$ lie on the open LHP, then, the satisfaction of one of two conditions, specifically when

- (k) at least one of the n zeros of $H|_{\mathbf{Q}}(s)$ is located on the open right half of the complex plane¹³ (RHP), or in case
 - (kk) the constant $K|_{\mathbf{Q}}$ features a negative sign,¹⁴
- directly ensures the truthfulness of condition (iv) from the Local Activity Theorem, which, in turn, proves the polarisation of the one-port on the Edge of Chaos at \mathbf{Q} . However, the satisfaction of either constraint (k) or constraint (kk) for the rational polynomial function $H|_{\mathbf{Q}}$ is only a sufficient condition for $\Re\{H|_{\mathbf{Q}}(j\omega)\}$ to go negative for some finite

¹³Given that, in view of Definition 4, Proposition 1, and Theorem 1 at page 3441 of [1], $H|_{\mathbf{Q}}(s)$ is locally-passive about a certain operating point \mathbf{Q} , iff $1/H|_{\mathbf{Q}}(s)$ is also locally-passive at \mathbf{Q} , in case the rational polynomial function from equation (47) features a zero with positive real part, $H|_{\mathbf{Q}}(s)$ is automatically locally-active at \mathbf{Q} . Moreover, providing, concurrently, all the poles of $H|_{\mathbf{Q}}(s)$ lie on the LHP, condition (iv) from the Local Activity Theorem necessarily applies for the rational polynomial function from equation (47) at \mathbf{Q} .

¹⁴If $K|_{\mathbf{Q}} < 0$, at least one of the coefficients in the polynomial at the numerator of $H|_{\mathbf{Q}}$, specifically the factor which multiplies s^n , is negative. As a result, $H|_{\mathbf{Q}}$ is not a positive real function [30], and, consequently, as descends from Theorem 1 at page 3441 of [1], is not locally passive at \mathbf{Q} . In view of the hypothesis, whereby all the roots of its denominator lie on the open LHP, this local transfer function is thus poised on the Edge of Chaos at the given operating point.

angular frequency ω_0 , under the hypothesis that all the roots of the denominator in (47) lie on the open LHP.

Referring to condition (k), at least one zero of the local input impedance $Z|_{\mathbf{Q}}(s)$ of the one-port from Fig. 1(a) about \mathbf{Q} lies on the open RHP if the sign of one or both of the two variable coefficients in the numerator of the rational polynomial function from equation (23) is negative. For a_1 to be negative, then, using equation (25), the inequality

$$R \cdot C_2 < 0 \quad (48)$$

should necessarily hold true. In order to ensure a negative-valued a_0 , employing equation (26), the fulfilment of condition

$$L \cdot C_2 < 0 \quad (49)$$

should be required. All in all, $Z|_{\mathbf{Q}}(s)$ has at least one zero on the open RHP if either (48) or (49) applies. Referring to condition (kk), the real factor K in the expression for $Z|_{\mathbf{Q}}(s)$ from equation (23) holds a negative polarity, if, using equation (24), the constraint

$$C_1 < 0 \quad (50)$$

is satisfied.

Choosing the common parameters of the two identical Chua circuits in Fig. 2, so as to poise each of them in a given operating point \mathbf{Q} , residing on the Edge of Chaos domain, it would be expected that, setting slightly-different initial conditions for the respective state vectors, while keeping them within the neighbourhood of \mathbf{Q} , after transients decay to zero, the two-cell array would asymptotically approach the homogeneous solution, with each of its constitutive units converging toward the same silent state, it would sit at, when let evolve on its own from the respective aforementioned starting point. However, the diffusion process may unexpectedly induce the *destabilisation of the array homogeneous solution*,¹⁵ resulting in the appearance of emergent phenomena, including an uncontrolled divergence of the physical variables of the reaction-diffusion network, or the formation of steady-state dynamic patterns of periodic or chaotic nature, across the homogeneous cellular medium itself, as foreseen by the Edge of Chaos Theorem from section II-B. In particular, Prigogine's Instability of the Homogeneous may be observed in the proposed RD-CNN from Fig. 2 under a sufficiently-low coupling resistance value, providing the operating point \mathbf{Q} of the one-port with access terminals A and B from Fig. 1(a) lies in the Edge of Chaos domain [1]. Despite the proposed Chua circuit parameter design procedure enables to poise each of the constitutive units of a given RD-CNN on some Edge of Chaos operating point \mathbf{Q} , whether dissipation-induced instabilities may truly appear across the resulting homogeneous medium may depend upon various factors, including array configuration, number of cells, number and kind of coupling ports, as well as diffusive coupling strength. The

¹⁵The mechanisms at the origin of diffusion-driven symmetry-breaking effects in homogeneous cellular media were extensively and intensively investigated for decades by luminaries of the calibre of Turing [17], Prigogine [22], and Smale [20].

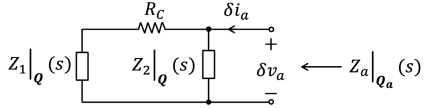


Fig. 6. Small-signal equivalent circuit model of the two-cell array. $Z_i|_Q \equiv Z|_Q$ denotes the local input impedance of the cell $i \in \{1, 2\}$, as seen from the respective coupling port, about some Edge of Chaos operating point \mathbf{Q} . $Z_a|_{Q_a}$ stands for the small-signal impedance of the RD-CNN, as observed across the terminals of either of its two constitutive units, when evaluated at the operating point $\mathbf{Q}_a = (\mathbf{Q}, \mathbf{Q})$ associated to the homogeneous solution.

following section derives the destabilization condition for the homogeneous solution of a simple RD-CNN, composed of two identical Chua circuits, offering one and only one coupling port, extracted across a capacitor, for the resistive coupling to the neighbouring cell.

C. III-C. Destabilization Condition for the Two-Cell Array Homogeneous Solution

Fig. 6 illustrates the small-signal equivalent circuit model of the two-cell array. The two cells are assumed to be identical, and biased on some common stable and locally-active operating point \mathbf{Q} . The local impedance¹⁶ $Z_i|_Q$ of the cell $i \in \{1, 2\}$ is thus equivalent to the closed-form expression for $Z|_Q$, as given in equation (23). The local impedance $Z_a|_{Q_a}$ of the RD-CNN, as it appears at the coupling port of either of its two constitutive units, e.g. cell 2 in the circuit schematic of Fig. 6, when computed about the operating point $\mathbf{Q}_a \triangleq (\mathbf{Q}, \mathbf{Q})$, which is associated to the array homogeneous solution, is found to assume the expression

$$\begin{aligned} Z_a|_{Q_a}(s) &= \frac{\mathcal{L}\{\delta v_a(t)\}}{\mathcal{L}\{\delta i_a(t)\}} \Big|_{Q_a} = \frac{N_a|_{Q_a}(s)}{D_a|_{Q_a}(s)} \\ &= Z_2|_Q(s) \parallel (Z_1|_Q(s) + R_C) \\ &= \frac{N|_Q(s) \cdot (N|_Q(s) + R_C \cdot D|_Q(s))}{D|_Q(s) (2 \cdot N|_Q(s) + R_C \cdot D|_Q(s))}, \end{aligned} \quad (51)$$

from which it is straightforward to infer the formulas for the numerator and denominator polynomials, indicated as $N_a|_{Q_a}(s)$, and $D_a|_{Q_a}(s)$, respectively, \parallel denotes the parallel operator from Circuit Theory [28], while $N|_Q(s)$ and $D|_Q(s)$ are in turn the numerator and denominator polynomials in the rational function from equation (23). The dissipation-induced destabilisation of the homogeneous solution of the simple RD-CNN is truly possible if and only if suitable choices for the coupling resistance R_C may allow to move to the RHP at least one of the poles of the sixth-order polynomial at the denominator of the array local impedance $Z_a|_{Q_a}(s)$, as seen from the coupling port of either cell, and evaluated at the operating point $\mathbf{Q}_a \triangleq (\mathbf{Q}, \mathbf{Q})$, which corresponds to the homogeneous solution of the cellular medium.

More specifically, since, as imposed earlier via inequalities (40)-(42), all the three roots of $D|_Q(s)$ lie on the open LHP, the stability of the denominator polynomial $D_a|_{Q_a}(s)$ in the

¹⁶The small-signal equivalent circuit model of Fig. 6 may be associated to the two-cell array configuration in Fig. 2 (Fig. 14(b)), upon assuming the local impedance $Z_i|_Q$ of the cell $i \in \{1, 2\}$ to appear across the coupling port $A_i - B_i$ ($\hat{A}_i - B_i$).

rational function from equation (51) depends merely upon the location of the roots of the third-order polynomial

$$\begin{aligned} &\frac{2 \cdot N|_Q(s) + R_C \cdot D|_Q(s)}{R_C} \\ &= s^3 + \rho_2|_Q \cdot s^2 + \rho_1|_Q \cdot s + \rho_0|_Q, \end{aligned} \quad (52)$$

where

$$\rho_2|_Q = 2 \cdot K \cdot G_C + b_2|_Q, \quad (53)$$

$$\rho_1|_Q = 2 \cdot K \cdot a_1 \cdot G_C + b_1|_Q, \text{ and} \quad (54)$$

$$\rho_0|_Q = 2 \cdot K \cdot a_0 \cdot G_C + b_0|_Q \quad (55)$$

assume strictly positive values. As a result, as it descends from the application of the Routh-Hurwitz stability criterion to the polynomial in equation (52), the homogeneous solution of the two-cell array may be destabilised if and only if the coupling conductance $G_C = R_C^{-1}$ may satisfy at least one of the three inequalities $\rho_2|_Q < 0$, $\rho_0|_Q < 0$, or $\rho_1|_Q \cdot \rho_2|_Q < \rho_0|_Q$ holds true, which, may be respectively reduced to

$$2 \cdot K \cdot G_C + b_2|_Q < 0, \quad (56)$$

$$2 \cdot K \cdot a_0 \cdot G_C + b_0|_Q < 0, \text{ and} \quad (57)$$

$$\begin{aligned} &G_C^2 + \frac{2 \cdot K (a_1 \cdot b_2|_Q + b_1|_Q - a_0)}{4 \cdot K^2 \cdot a_1} \\ &\cdot G_C + \frac{b_1|_Q \cdot b_2|_Q - b_0|_Q}{4 \cdot K^2 \cdot a_1} < 0. \end{aligned} \quad (58)$$

Importantly, in case the uncoupled cell is poised on some Edge of Chaos operating point, while, concurrently, neither of conditions (k) and (kk) from section III-B applies, i.e. none of conditions (48), (49), and (50) holds true, the first two inequalities from the set (56)-(58) never hold true, while the left hand side in the inequality (58) may go negative, under suitable coupling strength conditions, providing that the polynomial $N|_Q(s)$ at the numerator of the rational function from equation (23), expressing the local impedance $Z|_Q$ of the single cell, as seen from the respective coupling port, about \mathbf{Q} , features a non-null coefficient a_0 (see also the appendix for a counter-example, where, for a two-cell array, with different coupling scheme as compared to the one analysed here, none of the three inequalities from the set (56)-(58) may ever apply, when the linear part is purely-passive).

We can now test the one-port with access terminals A and B from the Chua circuit in Fig. 1(a) for Edge of Chaos for all possible parameter setting scenarios in case studies¹⁷ A, B, and C. In our in-depth analysis, aimed to explore the parameter space of either of the two one-ports, under study in the paper,¹⁸ in search for the respective Edge of Chaos domain, about a given admissible operating point, condition (iv) from the Local Activity Theorem was imposed once together with the disjunction between conditions (k) and (kk), and once assuming that none of these two constraints held true. Very importantly, only in the latter case, i.e. when with reference

¹⁷With reference to Table I, cases A and C were found to bifurcate into a pair of sub-cases each. In our classification convention, the sub-case 1 (2) was assigned to the cell parameter setting, allowing a positive (negative) value for the capacitor C_1 .

¹⁸Specifically, the body (appendix) of this manuscript focuses on the one-port with access terminals A and B (\hat{A} and B) from Fig. 1(a) (14(a)).

to the formula for the one-port local impedance, all the zeros and poles lie on the open LHP, while, concurrently, the real factor at the numerator is strictly positive, does our theoretical analysis allow the assignment of strictly-positive values to capacitances C_1 and C_2 , inductance L , and resistance R in each of the two identical Chua circuits, so as to poised them on some common stable and locally-active operating point, before the modulation of a resistive path, established to couple them, may induce the appearance of diffusion-driven instabilities across the resulting homogeneous medium, as long as the constraint, established by equation (58), holds true.

D. III-D. Testing the One-Port for Edge of Chaos

The discussion¹⁹ begins in section III-D-I with the results of the investigation of the most interesting case study, classified as A in section III-A.

1) *III-D-I Case Study A:* The results, presented in this section, are based upon the hypothesis (17), as well as upon the assumptions (3) and (13). The cell is poised on the Edge of Chaos at each of the two off-the-origin operating points \mathbf{Q}_- and \mathbf{Q}_+ , while, concurrently, its operating point \mathbf{Q}_0 in the origin of the three-dimensional state space of the ODE system (4)-(6) is unstable,²⁰ under either of three sets of conditions, i.e.

$$0 < C_1 < 2 \cdot C_2 \cdot (1 + g_1 \cdot R) < -C_2, \quad (59)$$

$$C_2 < 0, \quad (60)$$

$$L < 0, \quad (61)$$

$$C_1 < \frac{L}{R} \cdot \left(2 \cdot g_1 + \frac{3}{R} \right) \cdot \left(1 - 2 \cdot \frac{C_2}{C_1} \cdot (1 + g_1 \cdot R) \right), \text{ and} \quad (62)$$

$$-\frac{1}{g_1} < R < -\frac{3}{2} \cdot \frac{1}{g_1}, \quad (63)$$

resulting in case A.1.A, or

$$C_1 > \frac{L}{R} \cdot \left(2 \cdot g_1 + \frac{3}{R} \right) \cdot \left(1 - 2 \cdot \frac{C_2}{C_1} \cdot (1 + g_1 \cdot R) \right) > 0, \quad (64)$$

$$C_2 > 0, \quad (65)$$

$$L > 0, \text{ and} \quad (66)$$

$$-\frac{1}{g_1} < R < -\frac{3}{2} \cdot \frac{1}{g_1}, \quad (67)$$

corresponding to case A.1.B, where none of the inequalities (48), (49), and (50) is true, and, as a result, the parameters of all the linear two-terminal circuit elements are allowed to assume positive values, or even

$$C_1 < 2 \cdot C_2 \cdot (1 + g_1 \cdot R) < 0, \quad (68)$$

¹⁹The procedure for testing the Chua circuit for Edge of Chaos calls for the solution of a large system of inequalities, as defined in sections III.B. The existence of a solution allows to identify regions of the cell parameter space, where the effects of the diffusion process may destabilise the homogeneous solution of the two-cell array. While requiring a large amount of calculations, this mathematical analysis, applied to either of case studies A, B, and C from section III-A, is rather systematic, and may be easily verified through ad hoc software programs. As a result, in order to ensure a good level of readability, this section reports only the results of our investigations.

²⁰Fig. 3(a) illustrates the cell operating point stability configuration here.

$$C_2 > 0, \quad (69)$$

$$L < 0, \quad (70)$$

$$C_1 > \frac{L}{R} \cdot \left(2 \cdot g_1 + \frac{3}{R} \right) \cdot \left(1 - 2 \cdot \frac{C_2}{C_1} \cdot (1 + g_1 \cdot R) \right), \quad (71)$$

$$L < 8 \cdot C_2 \cdot R \cdot \frac{1 + g_1 \cdot R}{2 \cdot g_1 + \frac{3}{R}}, \text{ and} \quad (72)$$

$$-\frac{1}{g_1} < R < -\frac{3}{2} \cdot \frac{1}{g_1}, \quad (73)$$

associated to case A.2.A (refer to Table I).

The cell is poised on the Edge of Chaos at \mathbf{Q}_0 , whereas both \mathbf{Q}_- and \mathbf{Q}_+ are unstable,²¹ in case the Chua circuit parameters are chosen in compliance with the set of constraints

$$C_1 < 0, \quad (74)$$

$$C_2 > 0, \text{ and} \quad (75)$$

$$L > 0, \quad (76)$$

defining case study A.2.B from Table I.

2) *III-D-II Case Study B:*

The hypothesis (18), together with the assumptions (3) and (13), hold true for the results reported in this section. The cell is poised on the Edge of Chaos at \mathbf{Q}_0 , while being unstable²² at either \mathbf{Q}_- and \mathbf{Q}_+ , upon the satisfaction of each inequality from the set

$$C_1 < 0, \quad (77)$$

$$C_2 < 0, \text{ and} \quad (78)$$

$$L < 0, \quad (79)$$

defining case study B from Table I.

3) *III-D-III Case Study C:* This section reports results associated to the hypothesis (19), and on the assumptions (3) and (13). The cell is poised on the Edge of Chaos at²³ \mathbf{Q}_0 , under each of three different sets of conditions, specifically

$$C_1 > 0, \quad (80)$$

$$C_2 < -C_1 \left(1 + \frac{C_1 \cdot R}{g_1 \cdot L} \right) \cdot \frac{1}{1 + g_1 \cdot R} < 0, \text{ and} \quad (81)$$

$$L < 0, \quad (82)$$

defining case study C.1.A, or

$$C_1 > -\frac{g_1 \cdot L}{R} \cdot \left(1 + \frac{C_2}{C_1} \cdot (1 + g_1 \cdot R) \right) > 0, \quad (83)$$

$$C_2 > 0, \text{ and} \quad (84)$$

$$L > 0, \quad (85)$$

defining case study C.1.B, in which conditions (48), (49), and (50) are invalid, and, consequently, the selection of purely-passive linear components is possible, or even

$$C_1 < 0, \quad (86)$$

²¹Here the cell features the operating point stability configuration shown in Fig. 3(b).

²²The operating point stability configuration, which the cell admits under these circumstances, is depicted in Fig. 4.

²³The operating point stability configuration, which the cell admits under these circumstances, is depicted in Fig. 5.

TABLE I

COMPLETE CLASSIFICATION OF THE PARAMETER SETTINGS, ENABLING TO POISE THE ONE-PORT WITH ACCESS TERMINALS A AND B FROM THE CHUA CIRCUIT OF FIG. 1(A) ON AN EDGE OF CHAOS OPERATING POINT \mathbf{Q} UNDER THE ASSUMPTIONS (3) AND (13), FOR CASE STUDIES A, B, AND C, ASSOCIATED WITH THE HYPOTHESES (17), (18), AND (19), RESPECTIVELY. HERE THE ACRONYM EOC (OP) DENOTES EDGE OF CHAOS (OPERATING POINT), WHILE \mathcal{D}_{EOC} INDICATES FOR EACH CASE STUDY THE CELL EDGE OF CHAOS DOMAIN, QUANTITATIVELY DEFINED THROUGH THE RESPECTIVE SET OF PARAMETER CONSTRAINTS, RESULTING FROM THE ANALYSIS REPORTED IN THE TEXT. THE CHUA CIRCUIT ADMITS A TRIPLET OF OPERATING POINTS IN CASE STUDIES A AND B. IN EITHER CASE A.1.A, OR A.1.B, OR EVEN A2.A – LOOK AT FIG. 3(A) – THE AFOREMENTIONED ONE-PORT IS LOCALLY ACTIVE AND UNSTABLE (LOCALLY ACTIVE AND STABLE) AT \mathbf{Q}_0 (AT EITHER \mathbf{Q}_- OR \mathbf{Q}_+). WITH REFERENCE TO EACH OF CASES A.2.B – CONSULT FIG. 3(B) – AND B.1 – REFER TO FIG. 4 – THE ONE-PORT UNDER FOCUS IS LOCALLY ACTIVE AND UNSTABLE (LOCALLY ACTIVE AND STABLE) AT EITHER \mathbf{Q}_- OR \mathbf{Q}_+ (AT \mathbf{Q}_0). FINALLY, FOR CASES C.1.A, C.1.B, AND C.2 – SEE FIG. 5 – THE TWO-TERMINAL ELEMENT WITH PORT A–B FROM FIG. 1(A) IS POISED ON THE EDGE OF CHAOS AT THE GLOBALLY ASYMPTOTICALLY STABLE OPERATING POINT \mathbf{Q}_0 . THE CONDITION FOR THE DESTABILISATION OF THE TWO-CELL ARRAY HOMOGENEOUS SOLUTION IS PROVIDED BY THE LOGICAL DISJUNCTION BETWEEN CONSTRAINTS (56)–(58)

Case Study	EOC OP	\mathcal{D}_{EOC}
A.1.A	$\mathbf{Q}_{-/+}$	(59)–(63)
A.1.B	$\mathbf{Q}_{-/+}$	(64)–(67)
A.2.A	$\mathbf{Q}_{-/+}$	(68)–(73)
A.2.B	\mathbf{Q}_0	(74)–(76)
B.1	\mathbf{Q}_0	(77)–(79)
C.1.A	\mathbf{Q}_0	(80)–(82)
C.1.B	\mathbf{Q}_0	(83)–(85)
C.2	\mathbf{Q}_0	(86)–(88)

$$0 < C_2 < -C_1 \left(1 + \frac{C_1 \cdot R}{g_1 \cdot L} \right) \cdot \frac{1}{1 + g_1 \cdot R}, \text{ and} \quad (87)$$

$$L < 4 \cdot C_2 \cdot R \cdot \frac{1 + g_1 \cdot R}{g_1} < 0, \quad (88)$$

defining case study C.2 (see Table I).

E. III-E. Numerical Validation Results

The numerical validation, providing evidence for the fundamental role of the Physics Law of the Edge of Chaos in the array homogeneous solution destabilisation shall be first provided for the most interesting case study from Table I, specifically A.2.A, defined through the set of constraints (68)–(72), under the hypothesis (17), and the assumptions (3)–(13). For a cell parameter setting, complying with all these conditions, specifically $C_1 = -5 \cdot 10^{-9} F$, $C_2 = 1 \cdot 10^{-9} F$, $L = -48.15 \cdot 10^{-3} H$, and $R = 1.7 \cdot 10^3 \Omega$, and choosing R_0 , g_1 , and g_3 , as specified in section III-A, Fig. 7(a) shows the asymptotic approach of the Chua circuit from Fig. 1(a) toward the locally-stable and locally-active operating point \mathbf{Q}_- (consult the respective caption for details on its coordinates) from a nearby initial condition. The uncoupled cell features a high degree of excitability, hidden behind a seemingly quiet state. Fig. 7(b) illustrates the emergence of the homogeneous solution across the homogeneous cellular medium of Fig. 2, in a scenario, where the resistance of the coupling resistor R_C was preliminarily set to $34 \cdot 10^3 \Omega$ (slightly different values were assigned to the voltage signals $v_{C_{1,1}}$ and $v_{C_{1,2}}$ at $t = 0$ s, but the initial condition in the state space of each cell was

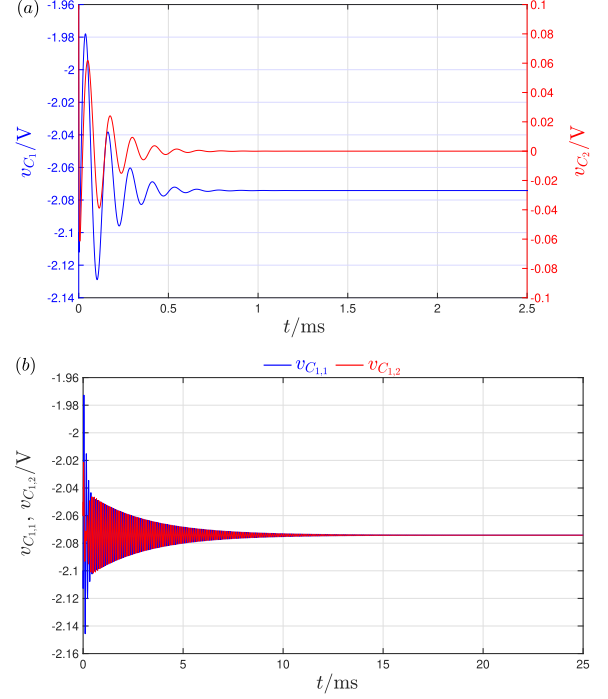


Fig. 7. (a) Convergence of the capacitor voltages v_{C_1} (blue trace), and v_{C_2} (red trace) in the basic cell, let evolve on its own from the initial condition $(v_{C_1}(0), v_{C_2}(0), i_L(0)) = (-2.1 \text{ V}, 0.1 \text{ V}, 1.2 \cdot 10^{-3} \text{ A})$, toward the levels, corresponding to the first and second coordinate of the stable and locally-active operating point $\mathbf{Q}_- = (V_{C_1,-}, V_{C_2,-}, I_{L,-}) = (-2.074 \text{ V}, 0 \text{ V}, 1.2 \cdot 10^{-3} \text{ A})$, respectively, as observed over the course of a numerical simulation of the third-order ODE system (4)–(6). (b) Numerical simulation of the sixth-order ODE set (7)–(12) from the initial condition $(v_{C_{1,1}}(0), v_{C_{2,1}}(0), i_{L,1}(0), v_{C_{1,2}}(0), v_{C_{2,2}}(0), i_{L,2}(0)) = (-2.1 \text{ V}, 0.1 \text{ V}, 1.2 \cdot 10^{-3} \text{ A}, -2.05 \text{ V}, 0.1 \text{ V}, 1.2 \cdot 10^{-3} \text{ A})$, revealing the approach of the voltages $v_{C_{1,1}}$ (blue trace), and $v_{C_{1,2}}$ (red trace), falling across the capacitor C_1 , sitting in cell 1 and in cell 2, respectively, toward the asymptotic value, which the capacitor voltage v_{C_1} was found to attain, in the numerical simulation of the basic cell from plot (a). The cell parameter set, specified for the simulations, which resulted in plots (a) and (b), reads as follows: $C_1 = -5 \cdot 10^{-9} \text{ F}$, $C_2 = 1 \cdot 10^{-9} \text{ F}$, $L = -48.15 \cdot 10^{-3} \text{ H}$, $R = 1.7 \cdot 10^3 \Omega$, $R_0 = 0 \Omega$, $g_1 = -0.75 \cdot 10^{-3} \Omega^{-1}$, and $g_3 = 37.6 \cdot 10^{-6} \Omega^{-1} \text{ V}^{-2}$. This set falls into the cell parameter region, classified as case study A.2.A from Table I. Additionally, a resistance of $34 \cdot 10^3 \Omega$ was assigned to the coupling resistor R_C for the numerical integration of the aforementioned sixth-order ODE system, which produced the illustration from plot (b).

displaced only a little from \mathbf{Q}_- , as may be inferred from the text in the relevant caption). Decreasing R_C further, while keeping the circuit parameter setting, and initial condition for each cell unchanged relative to the numerical simulation, which resulted in Fig. 7(b), for a sufficiently strong coupling condition, specifically as soon as R_C decreases down to $32.48 \cdot 10^3 \Omega$, rather than converging toward a common operating point, specifically \mathbf{Q}_- , the two identical cells are found to exhibit distinct dynamic behaviours, after transients vanish. In fact, for such coupling resistance bifurcation value, obtainable precisely from the destabilisation inequality (58), a dynamic pattern is found to appear across the homogeneous cellular medium at the expenses of the homogeneous solution. This is what Prigogine addressed as Instability of the Homogeneous in his classic book [23]. The two-cell array homogeneous solution keeps unstable for any value, assigned to the coupling resistance, below the bifurcation point, as predicted mathematically by imposing the logical

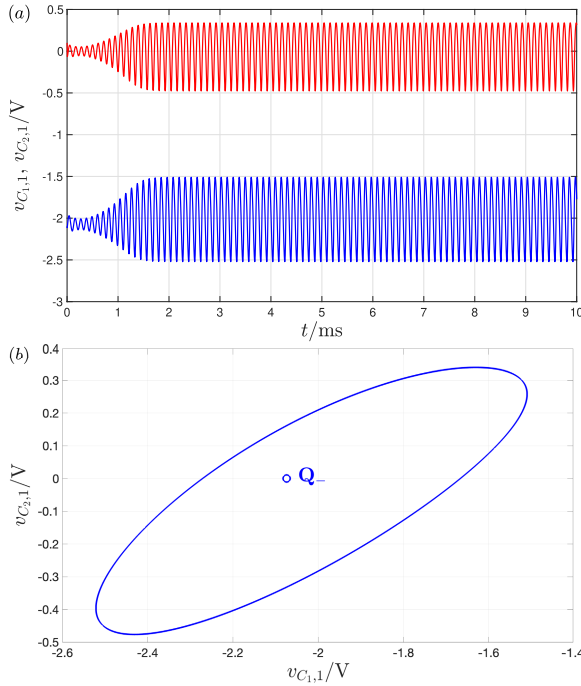


Fig. 8. (a) Blue (red) trace: time course of the voltage $v_{C1,1}$ ($v_{C2,1}$) across the capacitor C_1 (C_2) from cell 1, as recorded from 0 s to 10 ms during a numerical simulation of the two-cell array, in which R_C was decreased down to $25 \cdot 10^3 \Omega$. (b) Projection of the period-one limit cycle-based attractor of the ODE system (7)-(12) on the $v_{C2,1}$ versus $v_{C1,1}$ plane. The off-the-origin operating point \mathbf{Q}_- , which the Chua circuit admits in the uncoupled case (see the caption of Fig. 7(a) for the numerical values of its coordinates), and which denotes the common asymptotic destination of each of the two resistively-coupled cells, when, under sufficiently weak coupling scenarios, the reaction-diffusion network supports the emergence of the homogeneous solution, is also projected on the same plane, and marked through a hollow circle to indicate its unstable nature here. The cell parameter setting and the initial condition for each of the six state variables were kept unchanged relative to the numerical simulation from Fig. 7(b) (consult the text in the respective caption for the details).

disjunction between the three destabilisation inequalities (56)-(58). For example, Fig. 8 shows the periodic oscillations, developing across the capacitors C_1 and C_2 in cell 1, for $R_C = 25 \cdot 10^3 \Omega$. Higher-order dynamical phenomena emerge across the two-cell array for lower R_C values. Particularly, Fig. 9 (10) reveals how, at steady state, the time waveforms of the solutions to the ODE set (7)-(12) produce trajectories in the corresponding sixth-order state space, which converge asymptotically toward a single (double) scroll chaotic attractor. Reducing the coupling resistance to a greater extent, at some point, specifically for $R_C < 16.99 \cdot 10^3 \Omega$, physical variables across the proposed RD-CNN are found to diverge to infinity, similarly as is the case in Turing's two-cell array [1], as depicted in Fig. 11 for $R_C = 16 \cdot 10^3 \Omega$. Fig. 12 visualises a bifurcation diagram, which provides the local maxima and local minima in the steady-state time waveform of the voltage across capacitor C_1 from cell 1, as recorded from the numerical integration of the aforementioned sixth-order ODE system for each R_C value, extracted from the set $[16.99 \cdot 10^3 \Omega, 50 \cdot 10^3 \Omega]$, in steps of 1Ω .

Remark 4: When condition (iv) from the Local Activity Theorem from section II-A applies without the concurrent satisfaction of either of conditions (k) and (kk) from section III-B – refer to case studies A.1.B and C.1.B from

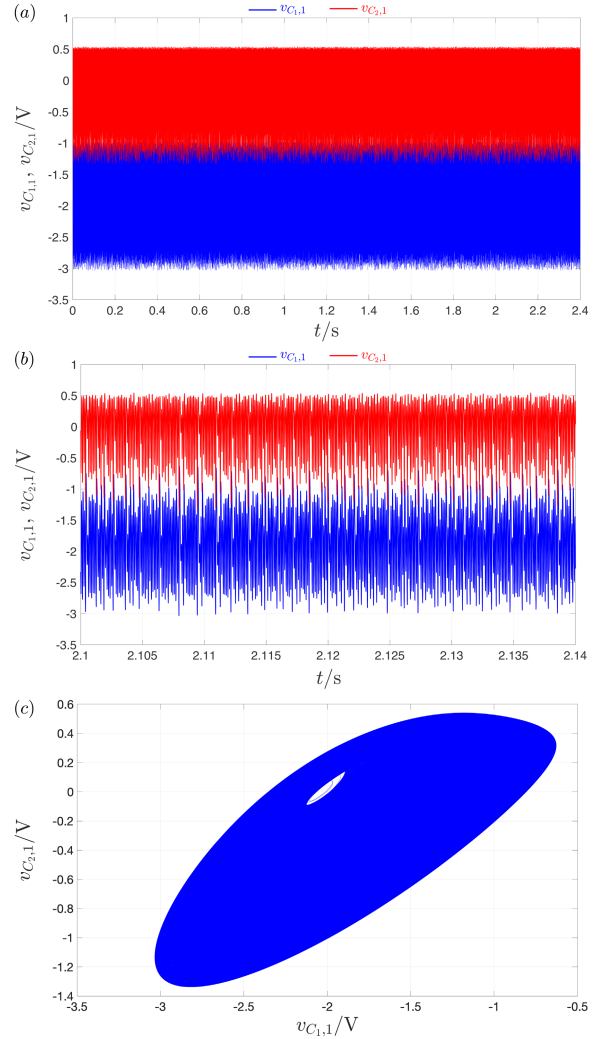


Fig. 9. (a) Evolution of the voltages $v_{C1,1}$ (blue trace), and $v_{C2,1}$ (red trace), respectively dropping across the capacitors C_1 and C_2 from cell 1, over the time interval $[0 \text{ s}, 2.4 \text{ s}]$, as resulting from a numerical integration of the ODE set (7)-(12), in which the resistance R_C of the coupling resistor was reduced to a value as small as $18 \cdot 10^3 \Omega$. (b) Closed-up view of the waveforms from (a), over the time interval $[2.1 \text{ s}, 2.14 \text{ s}]$, allowing to appreciate clearly the chaotic nature of the oscillatory voltages, which fall across the capacitors in this scenario. (c) Projection of the single-scroll chaotic attractor of the coupled system on the $v_{C2,1}$ versus $v_{C1,1}$ plane. Here the cell parameter setting and the initial condition for the numerical simulation of the reaction-diffusion network of Fig. 2 are the same as specified for the derivation of plot (b) from Fig. 7 (the corresponding caption reports the details).

Table I – the linear part of the RD-CNN is purely passive. Here, inequalities (56)-(57) never apply, and, providing that the last possible destabilisation condition, i.e. the constraint²⁴ (58), holds true, symmetry-breaking effects are found to result

²⁴In case study A.1.B from Table I, the inequality (58) reduces to $R \cdot C_1^2 - L \cdot (2 \cdot g_1 + 3/R) \cdot (C_1 - 2 \cdot C_2 \cdot (1 + g_1 \cdot R)) < 2 \cdot G_C \cdot L \cdot (5 \cdot C_2 + 4 \cdot g_1 \cdot R \cdot C_2 - C_1 - 2 \cdot G_C \cdot R \cdot C_2)$, where, since the left hand side is strictly positive in view of equation (64), $5 \cdot C_2 + 4 \cdot g_1 \cdot R \cdot C_2 - C_1 - 2 \cdot G_C \cdot R \cdot C_2$ must necessarily be larger than 0 as well. Using the values for C_1 , C_2 , L , and R , as specified in the caption of Fig. 13(a), the analysis precisely predicts instability for the homogeneous solution of the two-cell array for $9.129 \text{ k}\Omega < R_C < 78.871 \text{ k}\Omega$. In case study C.1.B from Table I, the inequality (58) reduces to $R \cdot C_1^2 + g_1 \cdot L(C_1 + C_2 \cdot (1 + g_1 \cdot R)) < 2 \cdot G_C \cdot L(-2 \cdot C_2 \cdot R \cdot G_C - C_1 - C_2 - 2 \cdot C_2 \cdot R \cdot g_1)$, where, in view of the positive polarity of the left hand side, descending from the inequality (83), the satisfaction of the inequality $-2 \cdot C_2 \cdot R \cdot G_C - C_1 - C_2 - 2 \cdot C_2 \cdot R \cdot g_1 > 0$ is also necessary. Using the values for C_1 , C_2 , L , and R , as specified in the caption of Fig. 13(b), the analysis precisely predicts instability for the homogeneous solution of the two-cell array for $2.877 \text{ k}\Omega < R_C < 99.041 \text{ k}\Omega$.

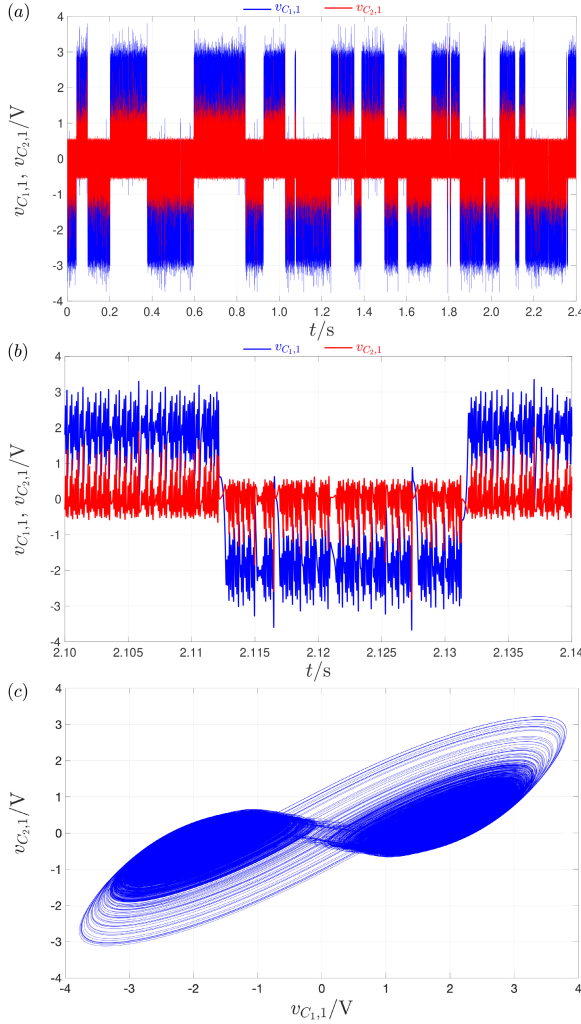


Fig. 10. (a) Oscillations in the capacitor voltages $v_{C_1,1}$ (blue trace), and $v_{C_2,1}$ (red trace) in cell 1 over the time interval $[0 \text{ s}, 2.4 \text{ s}]$ for $R_C = 17 \cdot 10^3 \Omega$. (b) Zoom-in visualisation of the signals from (a) over the time frame $[2.1, 2.14]\text{s}$, providing evidence for their chaotic behaviours. (c) Projection of the double-scroll chaotic attractor onto the $v_{C_2,1}$ versus $v_{C_1,1}$ plane. The cell parameter values and the initial conditions, assigned to the state variables, for the numerical integration of the sixth-order ODE set (7)-(12) are identical as indicated in the caption associated to Fig. 7(b).

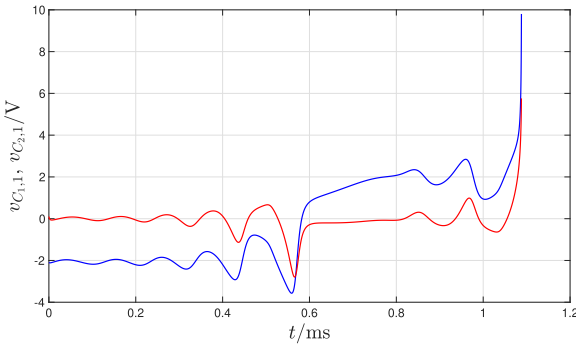


Fig. 11. Transient phase in the dynamical behaviour of the capacitors' voltages in cell 1 from $t = 0$ s to $t = 1.088$ ms, when convergence issues affect the numerical integration of the ODE set (7)-(12), signalling the ongoing divergence of its solution, for $R_C = 16 \cdot 10^3 \Omega$. Details on all the other parameters' values as well as on the initial conditions for the dynamic elements in the reaction-diffusion array are reported in the caption of Fig. 7(b).

in the emergence of regular periodic oscillations across the homogeneous cellular medium, only, as demonstrated, as

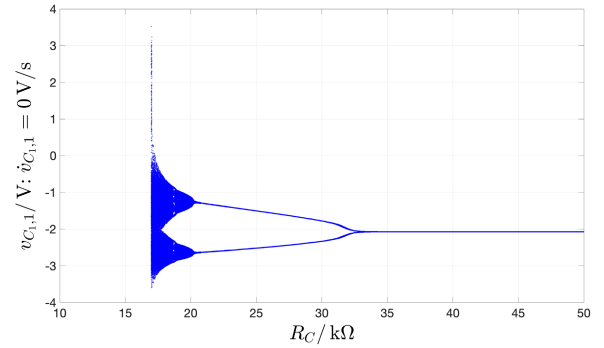


Fig. 12. Locus of points illustrating any local maximum or minimum in the steady-state time waveform of the voltage across capacitor C_1 from cell 1 in the reaction-diffusion array from Fig. 2 for each coupling resistance, falling in the range $[16.99 \cdot 10^3 \Omega, 50 \cdot 10^3 \Omega]$, and spaced from either the preceding or the successive R_C values by 1Ω (refer to the caption of Fig. 7(b) for the parameter setting, assigned to each of the two identical Chua circuits, as well as for the initial condition for the ODE set (7)-(12)). In the region, where the locus exhibits a unique branch, the two-cell array admits the homogeneous solution. When two branches appear in the bifurcation diagram, the array of resistively-coupled Chua circuits undergoes sustained period-1 limit-cycle oscillations ([31], [32]). The chaotic windows neatly stand out, being characterised by dense clouds of data points. In each case, when chaotic oscillations of large amplitude develop across the autonomous coupled system, which results in the appearance of a double scroll chaotic attractor in the six-dimensional state space of the ODE system (7)-(12), the bifurcation diagram features a set of points, which cover a wide interval of ordinate values, while stretching vertically in correspondence to the respective R_C value. Finally, for R_C values smaller than the lower bound in the range under sweep, physical variables in the reaction-diffusion array are found to diverge to infinity, which explains the lack of points in the leftmost region of the bifurcation diagram.

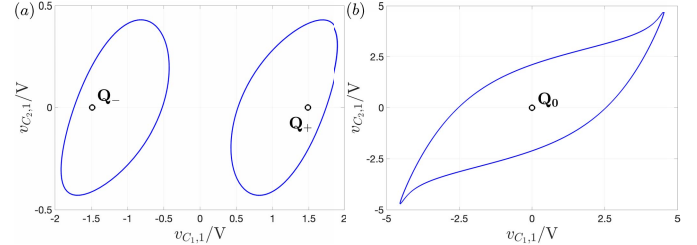


Fig. 13. Projection of the limit-cycle oscillations, which develop, upon a suitable coupling strength condition, across the two-cell array, onto the two-dimensional $v_{C_2,1}$ versus $v_{C_1,1}$ plane, in two distinct scenarios, respectively referring to cases A.1.B (a) and C.1.B (b) from Table I, where all the linear components, in each of the two identical Chua circuits, preliminarily biased on the Edge of Chaos about either of the off-the-origin operating points (about the operating point in the origin) are passive. Plot (a), revealing the existence of two locally-stable inhomogeneous dynamic patterns across the RD-CNN, was obtained through a couple of numerical simulations of the two-cell array from Fig. 2, upon choosing the linear circuit parameters in each Chua circuit as $C_1 = 2 \cdot 10^{-9} \text{ F}$, $C_2 = 15 \cdot 10^{-9} \text{ F}$, $L = 2 \cdot 10^{-3} \text{ H}$, and $R = 1.5 \cdot 10^3 \Omega$, and setting the coupling resistance as $R_C = 15 \cdot 10^3 \Omega$. In particular, the left (right) closed orbit in plot (a) was observed upon fixing the initial conditions as $(v_{C_1,1}(0), v_{C_2,1}(0), i_{L,1}(0)) = (-(+)\text{1.4887 V}, 0 \text{ V}, +(-)\text{9.9249} \cdot 10^{-4} \text{ A})$, and $(v_{C_1,1}(0), v_{C_2,1}(0), i_{L,1}(0)) = (-(+)\text{1.4887 V}, 0.1 \text{ V}, +(-)\text{9.9249} \cdot 10^{-4} \text{ A})$, for the first and second cell, respectively. The simulation result in (b) follows from a numerical integration of the sixth-order ODE (7)-(12) for $C_1 = 1 \cdot 10^{-9} \text{ F}$, $C_2 = 50 \cdot 10^{-9} \text{ F}$, $L = 0.5 \cdot 10^{-3} \text{ H}$, $R = 1.3 \cdot 10^3 \Omega$, and $R_C = 50 \cdot 10^3 \Omega$, and with $(v_{C_1,1}(0), v_{C_2,1}(0), i_{L,1}(0)) = (0 \text{ V}, 0 \text{ V}, 0 \text{ A})$, and $(v_{C_1,2}(0), v_{C_2,2}(0), i_{L,2}(0)) = (0.1 \text{ V}, 0 \text{ V}, 0 \text{ A})$. Plot (a) ((b)) depicts also the Edge of Chaos operating points (point), which each of the two identical cells features, in the uncoupled case, and which turns unstable, as the RD-CNN cells are let interact through a diffusion process.

second (third) numerical validation example from this section, in plot (a) ((b)) of Fig. 13 for a scenario from case study A.1.B (C.1.B), in which the diffusion process destabilises each of the

two identical cells from the common stable and locally-active operating point, specifically either \mathbf{Q}_- or \mathbf{Q}_+ (\mathbf{Q}_0).

IV. CONCLUSION

Emergent phenomena in homogeneous cellular media, including biological reaction-diffusion networks, are not possible unless the basic unit of arrays of this kind operates on the Edge of Chaos regime. Very recently, Cellular Neural Networks, leveraging the exceptional capability of certain miniaturised volatile memristors [18] to act as local sources of energy in the neighborhood of specific operating points, have been found to undergo diffusion-induced instabilities, leading to the formation of static [16] and dynamic periodic [19] patterns across the respective homogeneous media. However, to the best of our knowledge, the literature reports no evidence for Cellular Neural Networks, in which symmetry-breaking effects, triggered, rather counterintuitively, by the energy dissipation in the resistive couplings among the cells, results in the emergence of higher-order dynamical phenomena across the respective homogeneous media. This manuscript presents a simple Reaction-Diffusion Cellular Neural Network, composed of two identical and resistively-coupled Chua's circuits [25], [26], which exhibits dissipation-induced high-order dynamics, including silence-to-chaos transitions, and unbounded behaviours, due to uncontrollable positive feedback mechanisms. The application of systematic methods from Circuit and System Theory²⁵ [34], Nonlinear Dynamics [4], Control Theory [29], and Local Activity Theory [1] allows to carry out a thorough exploration of the parameter space of the basic reaction cell, so as to identify quantitatively the boundaries of the regions, within which the cell itself operates on the Edge of Chaos on its own, which is the Conditio Sine Qua Non for the emergence of dissipation-induced symmetry breaking effects, what Prigogine named Instability of the Homogeneous, with the consequent development of dynamical phenomena, including high-order chaotic oscillations, across the cellular array, upon the satisfaction of at least one of three ad hoc conditions for the destabilisation of the homogeneous solution. All in all, this manuscript clearly demonstrates how instrumental is to recur to the robust theoretical foundations of the Physics Principle of the Edge of Chaos to facilitate the quest for the seed of complexity in excitable media, a task which would be as prohibitive as searching for a needle in a haystack, otherwise.

APPENDIX: PRIGOGINE'S INSTABILITY OF THE HOMOGENEOUS IN THE TWO-CELL RD-CNN WITH ALTERNATIVE COUPLING ARRANGEMENT

Adopting the same circuit topology for the reaction cell (refer to Fig. 1(a)) as for the design of the RD-CNN from

²⁵The powerful analysis methods from Circuit and System Theory enable to gain a deep understanding of the operating principles of nonlinear physical media, such as the nano-devices under thorough exploration nowadays to enable a sustainable progress in integrated circuit electronics beyond the Moore era, as revealed in a recent scientific publication [33], which uncovered the physical mechanisms behind the emergence of fading memory effects in a resistance switching memory from the research group of Rainer Waser and Stephan Menzel.

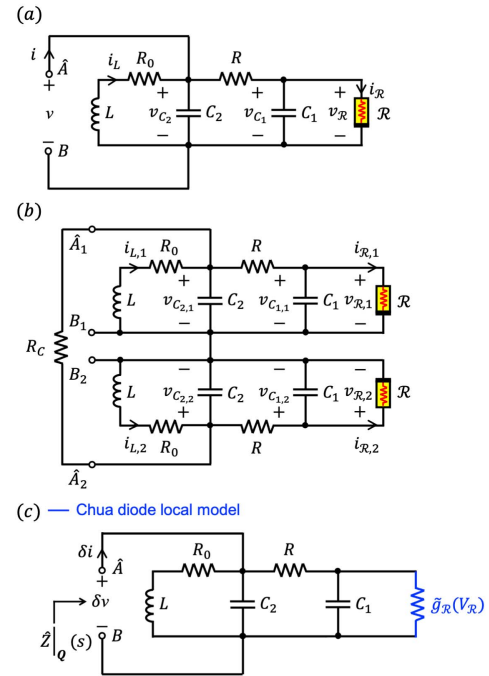


Fig. 14. (a) The Chua circuit. Terminals \hat{A} and B form the port to be employed for coupling diffusively two identical copies of such a reaction cell. (b) Array of identical Chua circuits coupled through the ports \hat{A}_1 - B_1 and \hat{A}_2 - B_2 . Differently from (Equivalently as in) the RD-CNN of Fig. 2, here the linear and passive resistor of resistance R_C is interposed between terminals \hat{A}_1 and \hat{A}_2 (terminals B_1 and B_2 are joined together). (c) Small-signal equivalent circuit model of the cell from (a), including a clear indication of the port, at which the local impedance $\hat{Z}|_Q(s)$ of the Chua circuit, about a given operating point Q , is computed.

Fig. 2, but employing a new port, specifically \hat{A} - B (see Fig. 14(a)) to couple resistively two identical copies of the cell itself, an alternative homogeneous cellular array, as shown in Fig. 14(b), is obtained. The sixth-order ODE system, governing the nonlinear dynamics of this alternative two-cell reaction-diffusion network topology, reads as

$$\frac{dv_{C1,1}}{dt} = \frac{1}{C_1} \cdot \left(\frac{v_{C2,1} - v_{C1,1}}{R} - i_{\mathcal{R},1}(v_{C1,1}) \right), \quad (89)$$

$$\frac{dv_{C2,1}}{dt} = \frac{1}{C_2} \cdot \left(i_{L,1} - \frac{v_{C2,1} - v_{C1,1}}{R} - \frac{v_{C2,1} - v_{C2,2}}{R_C} \right), \quad (90)$$

$$\frac{di_{L,1}}{dt} = \frac{1}{L} \cdot (-R_0 \cdot i_{L,1} - v_{C2,1}), \quad (91)$$

$$\frac{dv_{C1,2}}{dt} = \frac{1}{C_1} \cdot \left(\frac{v_{C2,2} - v_{C1,2}}{R} - i_{\mathcal{R},2}(v_{C1,2}) \right), \quad (92)$$

$$\frac{dv_{C2,2}}{dt} = \frac{1}{C_2} \cdot \left(i_{L,2} - \frac{v_{C2,2} - v_{C1,2}}{R} + \frac{v_{C2,1} - v_{C2,2}}{R_C} \right), \text{ and} \quad (93)$$

$$\frac{di_{L,2}}{dt} = \frac{1}{L} \cdot (-R_0 \cdot i_{L,2} - v_{C2,2}), \quad (94)$$

Fig. 14(c) depicts the small-signal equivalent circuit model of the basic cell from (a).

Applying standard circuit-theoretic principles to this local circuit model in the Laplace domain, the small-signal impedance $\hat{Z}|_Q(s)$ of the one-port with access terminals \hat{A} and B from Fig. 14(a) about a given operating point Q is

found to assume the following form

$$\hat{Z}|_{\mathbf{Q}(s)} = \frac{\hat{N}|_{\mathbf{Q}(s)}}{\hat{D}|_{\mathbf{Q}(s)}} = \hat{K} \cdot \frac{s^2 + \hat{a}_1|_{\mathbf{Q}} \cdot s + \hat{a}_0|_{\mathbf{Q}}}{s^3 + b_2|_{\mathbf{Q}} \cdot s^2 + b_1|_{\mathbf{Q}} \cdot s + b_0|_{\mathbf{Q}}}, \quad (95)$$

from which it is simple to infer the formulas for the numerator and denominator polynomials, referred to as $\hat{N}|_{\mathbf{Q}(s)}$ and $\hat{D}|_{\mathbf{Q}(s)}$, respectively,

$$\hat{K} \triangleq \frac{1}{C_2}, \quad (96)$$

$$\hat{a}_1|_{\mathbf{Q}} \triangleq \frac{1 + \tilde{g}\mathcal{R} \cdot R}{C_1 \cdot R}, \text{ and} \quad (97)$$

$$\hat{a}_0|_{\mathbf{Q}} \triangleq 0, \quad (98)$$

while the formulas for $b_2|_{\mathbf{Q}}$, $b_1|_{\mathbf{Q}}$, and $b_0|_{\mathbf{Q}}$ are provided in equations (27), (28), and (29), respectively, implying $\hat{D}|_{\mathbf{Q}(s)} \equiv D|_{\mathbf{Q}(s)}$. Computing the real part of $\hat{Z}|_{\mathbf{Q}(s)}$ for $s = j\omega$ yields

$$\Re\{\hat{Z}|_{\mathbf{Q}(j\omega)}\} = \frac{\hat{c}_4|_{\mathbf{Q}} \cdot \omega^4 + \hat{c}_2|_{\mathbf{Q}} \cdot \omega^2}{\omega^6 + d_4|_{\mathbf{Q}} \cdot \omega^4 + d_2|_{\mathbf{Q}} \cdot \omega^2 + d_0|_{\mathbf{Q}}}, \quad (99)$$

where

$$\hat{c}_4|_{\mathbf{Q}} \triangleq \hat{K} \cdot (b_2|_{\mathbf{Q}} - \hat{a}_1|_{\mathbf{Q}}), \text{ and} \quad (100)$$

$$\hat{c}_2|_{\mathbf{Q}} \triangleq \hat{K} \cdot (\hat{a}_1|_{\mathbf{Q}} \cdot b_1|_{\mathbf{Q}} - b_0|_{\mathbf{Q}}), \quad (101)$$

whereas the closed-form expressions for $d_4|_{\mathbf{Q}}$, $d_2|_{\mathbf{Q}}$, and $d_0|_{\mathbf{Q}}$ are respectively reported in equations (34), (35), and (36). Inspecting the numerator in equation (99), $\Re\{\hat{Z}|_{\mathbf{Q}(j\omega)}\}$ certainly admits two coincident zeros at angular frequencies

$$\omega_{1,2}|_{\Re\{\hat{Z}|_{\mathbf{Q}(j\omega)}\}=0} = 0 \text{ s}^{-1}, \quad (102)$$

whereas it vanishes at

$$\omega_{3,4}|_{\Re\{\hat{Z}|_{\mathbf{Q}(j\omega)}\}=0} = \mp\sqrt{\xi|_{\mathbf{Q}}}, \quad (103)$$

on condition that

$$\xi|_{\mathbf{Q}} \triangleq -\hat{c}_2|_{\mathbf{Q}}/\hat{c}_4|_{\mathbf{Q}} \quad (104)$$

is strictly positive. We are now in a position to list the conditions to be enforced on the parameters of the Chua circuit from Fig. 14(a), so as to drive the one-port with access terminals \hat{A} and B , extracted from the circuit itself, into the Edge of Chaos domain²⁶ (refer to section II-A). First of all, as follows from the Routh-Hurwitz stability criterion, in order for a given operating point \mathbf{Q} of this reaction cell, to exhibit asymptotic stability, the simultaneous satisfaction of three inequalities, involving the variable coefficients of the denominator $\hat{D}|_{\mathbf{Q}(s)}$ of $\hat{Z}|_{\mathbf{Q}(s)}$ – refer to equation (95) – and reading as $b_2|_{\mathbf{Q}} > 0$, $b_0|_{\mathbf{Q}} > 0$, and $b_1|_{\mathbf{Q}} \cdot b_2|_{\mathbf{Q}} > b_0|_{\mathbf{Q}}$, respectively, is necessary. Additionally, for the reaction cell to be locally active, $\Re\{\hat{Z}|_{\mathbf{Q}(j\omega)}\}$

²⁶As reported in Table II, cases A, B, and C were found to bifurcate into a pair of sub-cases each. As was the case in Table I, in our classification convention, the sub-case 1 (2) was assigned to the cell parameter setting, allowing a positive (negative) value for the capacitor C_1 .

has to go negative for at least one finite real-valued angular frequency $\omega = \omega_0$. Analysing equation (99), it turns out that

$$\Re\{\hat{Z}|_{\mathbf{Q}(j\omega)}\} < 0$$

$$\begin{cases} \text{for all } \omega \in (-\infty, \infty) \text{ if } \xi|_{\mathbf{Q}} < 0 \text{ and } \hat{c}_2|_{\mathbf{Q}} < 0, \\ \text{for } |\omega| < \sqrt{\xi|_{\mathbf{Q}}} \text{ if } \xi|_{\mathbf{Q}} > 0 \text{ and } \hat{c}_2|_{\mathbf{Q}} < 0, \text{ and} \end{cases} \quad (105)$$

$$\begin{cases} \text{for } |\omega| > \sqrt{\xi|_{\mathbf{Q}}} \text{ if } \xi|_{\mathbf{Q}} > 0 \text{ and } \hat{c}_2|_{\mathbf{Q}} > 0. \end{cases} \quad (107)$$

As discussed in the body of the manuscript for the one-port with access terminals A and B , shown in Fig. 1(a), the exploration of the parameter space of the Chua circuit in search for the Edge of Chaos domain of the one-port with access terminals A and B , depicted in Fig. 14(a), is carried out under the hypothesis that the satisfaction of the constraints (105)-(107), i.e. of condition (iv) from the Local Activity Theorem from section II-A, occurs once together and once without the truthfulness of the logical disjunction between two conditions (k) and (kk) from section III-B, which, here, respectively reduce to the inequalities $\hat{a}_1|_{\mathbf{Q}} < 0$, and $\hat{K} < 0$. As was the case in the coupling configuration of the two-cell array from Fig. 2, the linear part of the RD-CNN is allowed to be purely-passive only in the latter case, where $\Re\{\hat{Z}|_{\mathbf{Q}(j\omega)}\}$ may go negative while none of the inequalities (105)-(107) holds true. Since, as was the case for the coupling arrangement in the RD-CNN of Fig. 2, the two constitutive units of the array of Fig. 14(b) are physically connected through one of their available ports only, the condition for the destabilisation of the homogeneous solution of the cellular system is still provided by the logical disjunction between inequalities (56), (57), and (58), upon the substitutions $K \rightarrow \hat{K}$, $a_1|_{\mathbf{Q}} \rightarrow \hat{a}_1|_{\mathbf{Q}}$, $a_0|_{\mathbf{Q}} \rightarrow \hat{a}_0|_{\mathbf{Q}}$. Importantly, as a clear difference from the object of the investigations in the body of the paper, here, when $\hat{a}_1|_{\mathbf{Q}} > 0$, and $\hat{K} > 0$, none of the inequalities (56)-(58) may ever hold true, since $\hat{a}_0|_{\mathbf{Q}} = 0$, as reported in equation (98), which implies that symmetry-breaking phenomena may never occur in the two-cell array, under focus in this appendix, when all the linear components in each of its identical constitutive units are drawn from the respective passive classes.

Having quantitatively defined the necessary conditions for the emergence of symmetry-breaking phenomena within the proposed RD-CNN, lengthy but straightforward calculations, omitted here to maintain a good degree of readability throughout the manuscript, enable to identify all the possible Chua circuit parameter regions, within which the one-port with access terminals \hat{A} and B , identifiable in Fig. 14(a), is poised on the Edge of Chaos, under the assumptions (3) and (13), and for each of the case studies A, B, and C, associated to hypotheses (17), (18), and (19), respectively. Importantly, in regard to the possible operating point stability patterns for the one-port with access terminals \hat{A} and B from Fig. 14(a), our investigations reveal that, unlike what is the case for the one-port from the same reaction cell, but with access terminals A and B , as indicated in Fig. 1(a), here there exists a unique admissible configuration in case²⁷ A, where, as visualised in Fig. 3(a),

²⁷Fig. 3(b), illustrating a possible operating point stability configuration for the one-port with access terminals A and B from Fig. 1(a) is not admissible, however, for the two-terminal element with port $\hat{A}-B$ from Fig. 14(a).

TABLE II

COMPLETE CLASSIFICATION OF THE PARAMETER SETTINGS, ENABLING TO DRIVE THE ONE-PORT WITH TERMINALS \hat{A} AND B FROM FIG. 14(A) INTO A EDGE OF CHAOS OPERATING POINT \mathbf{Q} UNDER THE ASSUMPTIONS (3) AND (13) IN CASE STUDIES A, B, AND C, WHICH ARE BASED UPON THE HYPOTHESES (17), (18), AND (19), RESPECTIVELY. HERE THE ACRONYM EOC (OP) DENOTES EDGE OF CHAOS (OPERATING POINT), WHILE \mathcal{D}_{EOC} INDICATES FOR EACH CASE STUDY THE CELL EDGE OF CHAOS DOMAIN, QUANTITATIVELY DEFINED THROUGH THE RESPECTIVE SET OF PARAMETER CONSTRAINTS, RESULTING FROM THE ANALYSIS REPORTED IN THE TEXT. THE CHUA CIRCUIT ADMITS A TRIPLET OF OPERATING POINTS IN CASE STUDIES A AND B. IN ANY OF THE FOUR CASES A.1.A, A.1.B, A2 – LOOK AT FIG. 3(A) – OR B.2 – REFER TO FIG. 15 – THE AFOREMENTIONED ONE-PORT IS LOCALLY ACTIVE AND UNSTABLE (LOCALLY ACTIVE AND STABLE) AT \mathbf{Q}_0 (AT EITHER \mathbf{Q}_- OR \mathbf{Q}_+). WITH REFERENCE TO CASE B.1 – SEE FIG. 4 – THE ONE-PORT UNDER STUDY IS LOCALLY ACTIVE AND UNSTABLE (LOCALLY ACTIVE AND STABLE) AT EITHER \mathbf{Q}_- OR \mathbf{Q}_+ (AT \mathbf{Q}_0). FINALLY, IN EITHER CASE C.1.A, OR C.1.B, OR EVEN C.2 – SEE FIG. 5 – THE TWO-TERMINAL ELEMENT WITH PORT $\hat{A}-B$ FROM FIG. 14(A) IS POISED ON THE EDGE OF CHAOS AT \mathbf{Q}_0 . THE DESTABILISATION CONDITION FOR THE TWO-CELL ARRAY HOMOGENEOUS SOLUTION IS PROVIDED ONCE AGAIN BY THE LOGICAL DISJUNCTION BETWEEN INEQUALITIES (56), (57), AND (58), UPON THE SUBSTITUTIONS $K \rightarrow \hat{K}$, $a_1 \rightarrow \hat{a}_1$, $a_0 \rightarrow \hat{a}_0$. NOTABLY, UNLIKE WHAT WAS THE CASE FOR THE COUPLING ARRANGEMENT, ANALYSED IN THE BODY OF THE PAPER, HERE, IN CASES A.1.B AND C.1.B, WHERE $\hat{K} > 0$, AND $\hat{a}_1 > 0$, NONE OF THE POSSIBLE DESTABILISATION CONDITIONS, ENCODED MATHEMATICALLY IN THE INEQUALITIES (56), (57), AND (58), RESPECTIVELY, MAY EVER HOLD TRUE, SINCE $\hat{a}_0 = 0$ (SEE EQUATION (98)), WHICH IMPLIES THAT THE HOMOGENEOUS SOLUTION OF THE TWO-CELL ARRAY FROM FIG. 14(B) MAY NEVER BE DESTABILISED BY DIFFUSION, WHEN ITS LINEAR PART IS PURELY PASSIVE (ON THE OTHER HAND, AS SHOWN IN PLOTS (A) AND (B) FROM FIG. 13, RESPECTIVELY, THE RD-CNN OF FIG. 2 SUPPORTS THE FORMATION OF INHOMOGENEOUS DYNAMIC PATTERNS, WHEN THE PARAMETERS OF ITS CELLS ARE SET ACCORDING TO THE CONSTRAINTS IN CASES A.1.B AND C.1.B FROM TABLE I)

Case Study	EOC OP	\mathcal{D}_{EOC}
A.1.A	$\mathbf{Q}_{-/+}$	(59)-(63)
A.1.B	$\mathbf{Q}_{-/+}$	(64)-(67)
A.2	$\mathbf{Q}_{-/+}$	(68)-(71), and (73)
B.1	\mathbf{Q}_0	(77)-(79)
B.2	$\mathbf{Q}_{-/+}$	(108)-(110)
C.1.A	\mathbf{Q}_0	(80)-(82)
C.1.B	\mathbf{Q}_0	(83)-(85)
C.2	\mathbf{Q}_0	(86)-(87), and (111)

\mathbf{Q}_- and \mathbf{Q}_+ are locally asymptotically stable operating points (\mathbf{Q}_0 is an unstable operating point) of $\hat{Z}|_{\mathbf{Q}}(s)$ from equation (95). On the other hand, a couple of possible schemes appear in case B, as respectively depicted in Figs. 4, and 15, where, in turn, the operating point in the origin (the off-the-origin operating points) of the one-port under focus in this appendix features global asymptotic stability (feature local asymptotic stability). With reference to case study C, analogously as was evinced from the analysis of $Z|_{\mathbf{Q}}(s)$ in equation (23) for the one-port of interest in the two-cell coupling arrangement assumed for the RD-CNN of Fig. 2, each of the poles of $\hat{Z}|_{\mathbf{Q}}(s)$ from equation (95) about \mathbf{Q}_0 may feature a negative real part, and, consequently, Fig. 5 still shows the only possible operating point stability configuration for the one-port under study here. Table II reports the boundaries of each of the parameter domains, endowing the one-port, featuring access terminals \hat{A} and B , and extracted from the Chua circuit of Fig. 14(a), with a high degree of excitability, which, hidden behind an apparently-quiet steady state, may vividly manifest itself, as the two-cell array from Fig. 14(b) reproduces the

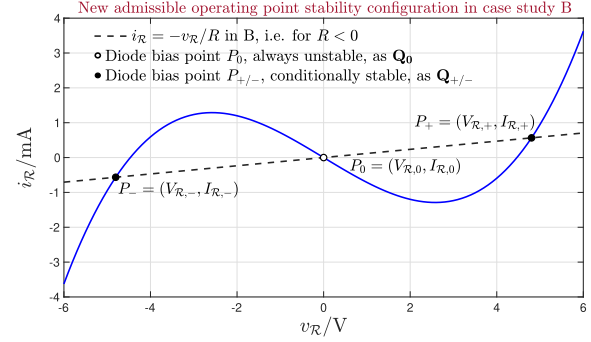


Fig. 15. Additional possible stability configuration for the operating points of the one-port with access terminals \hat{A} and B from the cell of Fig. 14(a), besides the one, depicted in Fig. 4, in case study B, i.e. under the hypothesis (18), and the assumptions (3) and (13). The solid blue trace shows the graph of the Chua diode constitutive relationship from equation (2) under the parameter setting reported in the caption of Fig. 3, whereas the dashed black line visualises the $i_R = -v_R/R$ versus v_R locus for $R = -8.5 \text{ k}\Omega$. On condition that each of the constraints, listed along row B.2 from Table II, holds true, the one-port under focus is locally active but unstable (is poised on the Edge of Chaos domain) at the operating point \mathbf{Q}_0 (at either of the off-the-origin operating points \mathbf{Q}_- and \mathbf{Q}_+), which corresponds to the diode bias points P_0 (which respectively correspond to the diode bias points P_- and P_+). The coordinates of the three admissible diode bias points in case study B are provided in the caption of Fig. 3.

counterintuitive complex phenomenon, referred to as Instability of the Homogeneous by Ilya Prigogine [22], [23], under relatively strong coupling conditions. In regard to case A, there exist three possible sets of conditions, involving the parameters of the Chua circuit-based reaction cell, which poise the one-port under study on the Edge of Chaos at either \mathbf{Q}_- or \mathbf{Q}_+ . The first, second, and third set, classified in turn as cases A.1.A, A.1.B, and A.2 in Table II, consists of constraints (59)-(63), (64)-(67), as well as²⁸ (68)-(71) and (73), respectively. As for case B, the one-port under focus is poised on the Edge of Chaos at \mathbf{Q}_0 if the inequalities (77)-(79) concurrently hold true, resulting in case B.1, or at either \mathbf{Q}_- or \mathbf{Q}_+ , provided the conditions

$$C_1 > 0, \quad (108)$$

$$C_2 < 0, \text{ and} \quad (109)$$

$$L < 0, \quad (110)$$

defining case B.2, simultaneously apply (consult Table II as well). Finally, analysing case C, the satisfaction of either of three systems of inequalities allows the one-port with access terminals \hat{A} and B from Fig. 14(a) to enter the Edge of Chaos domain at \mathbf{Q}_0 , namely either (80)-(82), grouped in case C.1.A, or (83)-(85), referred to as case C.1.B, or even (86)-(87), and²⁹

$$L < 0, \quad (111)$$

classified as case C.2 (see also Table II). Differently from what is the case for the two-cell array, examined in the body

²⁸Unlike what occurs in the corresponding case – specifically A.2.A from Table I – from the two-cell coupling arrangement, inferable from the ODE set (7)-(12), the inequality (72) is unnecessary for case A.2 (see Table II).

²⁹Differently from the corresponding case, specifically C.2, from Table I, in the two-cell coupling arrangement, envisaged by the sixth-order ODE set (89)-(94), the constraint (88) reduces to a simpler condition, as reported in equation (111) (consult Table II).

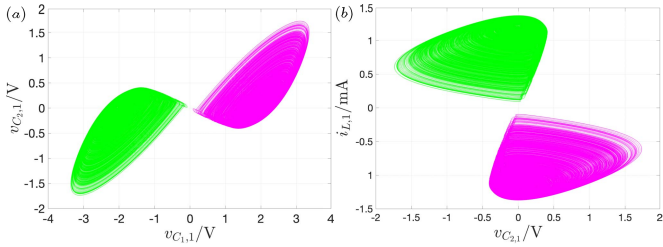


Fig. 16. Bistability in the dynamics of the autonomous dynamic system described by the sixth-order ODE system (89)-(94) for $R_C = 10 \cdot 10^3 \Omega$. The green (magenta) locus in plot (a) (b) shows the projection of the single-scroll chaotic attractor, appearing at the end of the transient phase, in the six-dimensional state space of the aforementioned ODE set, on the $v_{C_2,1}$ ($v_{C_1,1}$) versus $i_{L,1}$ ($v_{C_2,1}$) plane, for initial conditions, assigned to the three-dimensional state vectors of the two cells, chosen, close one to the other, from the neighborhood of \mathbf{Q}_- (\mathbf{Q}_+), i.e. as $v_{C_1,1}(0) = -(+)\cdot 2.1 \text{ V}$, $v_{C_2,1}(0) = 0.1 \text{ V}$, $i_{L,1}(0) = +(-)\cdot 1.2 \text{ mA}$, $v_{C_1,2}(0) = -(+)\cdot 2.05 \text{ V}$, $v_{C_2,2}(0) = 0.1 \text{ V}$, and $i_{L,2}(0) = +(-)\cdot 1.2 \text{ mA}$. The circuit parameter setting for each of the two identical cells of the RD-CNN from Fig. 14(b) reads as follows: $C_1 = -5 \cdot 10^{-9} \text{ F}$, $C_2 = 1 \cdot 10^{-9} \text{ F}$, $L = -48.15 \cdot 10^{-3} \text{ A}$, $R = 1.7 \cdot 10^3 \Omega$, $R_0 = 0 \Omega$, $g_1 = -0.75 \cdot 10^{-3} \Omega^{-1}$, and $g_3 = 37.6 \cdot 10^{-6} \Omega^{-1} \cdot \text{V}^{-2}$. For this cell parameter set, falling in case A.2 from Table II, with reference to the three-dimensional state space of the ODE set (4)-(6), $\mathbf{Q}_- = (V_{C_1,-}, V_{C_2,-}, I_{L,-})$ ($\mathbf{Q}_+ = (V_{C_1,+}, V_{C_2,+}, I_{L,+})$) lies at $(-(+)\cdot 2.0742 \text{ V}, 0 \text{ V}, +(-)\cdot 1.2 \text{ mA})$.

of the paper (recall Figs. 13(a) and (b)), the observation of diffusion-driven instabilities in the network of Fig. 14(b) requires the use of at least one active one-port per cell from the set of three two-terminal linear dynamic elements C_1 , C_2 , and L . Choosing the same set of circuit parameters for each of the two identical cells in Fig. 14(a), as specified for the first numerical validation example from section III-E, particularly $C_1 = -5 \cdot 10^{-9} \text{ F}$, $C_2 = 1 \cdot 10^{-9} \text{ F}$, $L = -48.15 \cdot 10^{-3} \text{ A}$, $R = 1.7 \cdot 10^3 \Omega$, $R_0 = 0 \Omega$, $g_1 = -0.75 \cdot 10^{-3} \Omega^{-1}$, and $g_3 = 37.6 \cdot 10^{-6} \Omega^{-1} \cdot \text{V}^{-2}$, which meets the conditions, associated to case study A.2 from Table II, as the coupling resistance is decreased down to the threshold of $15.569 \cdot 10^3 \Omega$, obtainable precisely from the solution of the destabilisation inequality (58), the homogeneous solution of the two-cell array, emerging for initial conditions, assigned to its constitutive units, chosen, close one to the other, and nearby either of the two Edge of Chaos operating points \mathbf{Q}_- or \mathbf{Q}_+ , loses stability, and, consequently, the ODE system (89)-(94) is found to exhibit an inhomogeneous dynamic pattern, after transients decay to zero. As mathematically predicted from the logical disjunction between the destabilisation inequalities (56)-(58), the homogeneous solution of the two-cell array keeps unstable for any coupling condition stronger than what is the case at the bifurcation point. As R_C is progressively reduced from the bifurcation threshold, the two-cell array is found to exhibit also some high-order dynamical behaviour, at steady state, including the convergence toward either of two coexisting locally stable single-scroll chaotic attractors, which, for $R_C = 10 \text{ k}\Omega$, are projected on the $v_{C_2,1}$ ($i_{L,1}$) versus $v_{C_1,1}$ ($v_{C_2,1}$) plane in plot (a) ((b)) of Fig. 16 (refer to the caption for more details).

REFERENCES

- [1] L. O. Chua, "Local activity is the origin of complexity," *Int. J. Bifurcation Chaos*, vol. 15, no. 11, pp. 3435–3456, 2005.
- [2] L. O. Chua, *The Chua Lectures: From Memristors and Cellular Nonlinear Networks to the Edge of Chaos, Volume IV. Local Activity Principle: Chua's Riddle, Turing Machine, and Universal Computing Rule 137* (World Scientific Series on Nonlinear Science Series A). Singapore: World Scientific, 2020.
- [3] K. Mainzer and L. O. Chua, *The Local Activity Principle*. London, U.K.: Imperial College Press, 2013.
- [4] S. Wiggins, *Introduction to Applied Nonlinear Dynamical Systems and Chaos* (Texts in Applied Mathematics), 2nd ed. New York, NY, USA: Springer, 2003.
- [5] L. Chua, V. Sbitnev, and H. Kim, "Neurons are poised near the edge of chaos," *Int. J. Bifurcation Chaos*, vol. 22, no. 4, Apr. 2012, Art. no. 1250098.
- [6] L. Chua, "Hodgkin-Huxley equations implies edge of chaos kernel," *Jpn. J. Appl. Phys.*, vol. 61, Oct. 2022, Art. no. SM0805.
- [7] L. O. Chua, Ed., *CNN: A Paradigm for Complexity* World Scientific Series on Nonlinear Science. Singapore: World Scientific, 1998.
- [8] M. D. Pickett and R. S. Williams, "Sub-100 fJ and sub-nanosecond thermally driven threshold switching in niobium oxide crosspoint nanodevices," *Nanotechnology*, vol. 23, no. 21, May 2012, Art. no. 215202.
- [9] A. Ascoli, S. Slesazeck, H. Mähne, R. Tetzlaff, and T. Mikolajick, "Nonlinear dynamics of a locally-active memristor," *IEEE Trans. Circuits Syst. I, Reg. Papers*, vol. 62, no. 4, pp. 1165–1174, Apr. 2015.
- [10] W. Yi, K. K. Tsang, S. K. Lam, X. Bai, J. A. Crowell, and E. A. Flores, "Biological plausibility and stochasticity in scalable VO2 active memristor neurons," *Nature Commun.*, vol. 9, no. 1, pp. 1–10, Dec. 2018.
- [11] I. Messaris et al., "NbO₂-Mott memristor: A circuit-theoretic investigation," *IEEE Trans. Circuits Syst. I, Reg. Papers*, vol. 68, no. 12, pp. 4979–4992, Dec. 2021.
- [12] A. S. Demirkol, A. Ascoli, I. Messaris, and R. Tetzlaff, "Pattern formation dynamics in a memristor cellular nonlinear network structure with a numerically stable VO2 memristor model," *Jpn. J. Appl. Phys.*, vol. 61, Oct. 2022, Art. no. SM0807, doi: [10.3548/1347-4065/ac8489](https://doi.org/10.3548/1347-4065/ac8489).
- [13] T. D. Brown, S. M. Bohaiuchuk, M. Islam, S. Kumar, E. Pop, and R. S. Williams, "Electro-thermal characterization of dynamical VO2 memristors via local activity modeling," *Adv. Mater.*, vol. 2022, Nov. 2022, Art. no. 2205451, doi: [10.1002/adma.202205451](https://doi.org/10.1002/adma.202205451).
- [14] L. Chua, V. Sbitnev, and H. Kim, "Hodgkin-Huxley axon is made of memristors," *Int. J. Bifurcation Chaos*, vol. 22, no. 3, Mar. 2012, Art. no. 1230011.
- [15] T. D. Brown, S. Kumar, and R. S. Williams, "Physics-based compact modeling of electro-thermal memristors: Negative differential resistance, local activity, and non-local dynamical bifurcations," *Appl. Phys. Rev.*, vol. 9, no. 1, Mar. 2022, Art. no. 011308, doi: [10.1063/5.0070558](https://doi.org/10.1063/5.0070558).
- [16] A. Ascoli, A. S. Demirkol, R. Tetzlaff, and L. Chua, "Edge of Chaos is sine Qua non for Turing instability," *IEEE Trans. Circuits Syst. I, Reg. Papers*, vol. 69, no. 11, pp. 4596–4609, Nov. 2022.
- [17] A. M. Turing, "The chemical basis of morphogenesis," *Phil. Trans. Roy. Soc. B*, vol. 237 no. 641, pp. 37–72, Aug. 1952.
- [18] A. Ascoli, A. S. Demirkol, R. Tetzlaff, S. Slesazeck, T. Mikolajick, and L. O. Chua, "On local activity and edge of chaos in a NaMLab memristor," *Frontiers Neurosci.*, vol. 15, Apr. 2021, Art. no. 651452, doi: [10.3389/fnins.2021.651452](https://doi.org/10.3389/fnins.2021.651452).
- [19] A. Ascoli, A. S. Demirkol, R. Tetzlaff, and L. Chua, "Edge of Chaos theory resolves Smale paradox," *IEEE Trans. Circuits Syst. I, Reg. Papers*, vol. 69, no. 3, pp. 1252–1265, Mar. 2022.
- [20] S. Smale, "A mathematical model of two cells via Turing's equation," in *The Hopf Bifurcation and Its Applications* (Lectures in Applied Mathematics), vol. 6. Providence, RI, USA: Amer. Math. Soc., 1974, pp. 15–26.
- [21] A. Ascoli, A. S. Demirkol, N. Schmitt, R. Tetzlaff, and L. O. Chua, "Edge of Chaos behind bistability of the inhomogeneous in homogeneous cellular media," in *Proc. IEEE Int. Conf. Metrol. Extended Reality, Artif. Intell. Neural Eng. (MetroXRAINE)*, Oct. 2022.
- [22] I. Prigogine and G. Nicolis, "On symmetry-breaking instabilities in dissipative systems," *J. Chem. Phys.*, vol. 46, no. 9, pp. 3542–3550, 1967.
- [23] I. Prigogine, *From Being to Becoming: Time and Complexity in the Physical Sciences*. San Francisco, NY, USA: W. H. Freeman & Co, 1980.
- [24] I. Prigogine and I. Stengers, *Order Out of Chaos: Man's New Dialogue With Nature*. New York, NY, USA: Bantam Dell Publishing Group, 1989.
- [25] M. P. Kennedy, "Three steps to Chaos. I. Evolution," *IEEE Trans. Circuits Syst. I, Fundam. Theory Appl.*, vol. 40, no. 10, pp. 640–656, Oct. 1993.

- [26] M. P. Kennedy, "Three steps to chaos. II. A Chua's circuit primer," *IEEE Trans. Circuits Syst. I, Fundam. Theory Appl.*, vol. 40, no. 10, pp. 657–674, Oct. 1993.
- [27] A. S. Demirkol, A. Ascoli, M. Weiher, and R. Tetzlaff, "Exact inductorless realization of Chua circuit using two active elements," *IEEE Trans. Circuits Syst. II, Exp. Briefs*, to be published.
- [28] L. O. Chua, C. A. Desoer, and E. A. Kuh, *Linear and Nonlinear Circuits*. New York, NY, USA: McGraw-Hill, 1987.
- [29] A. Hurwitz, "On the conditions under which an equation has only roots with negative real parts," *Sel. Papers Math. Trends Control Theory*, vol. 46, no. 2, pp. 273–284, 1964.
- [30] E. A. Guillemin, *Synthesis of Passive Networks: Theory and Methods Appropriate to the Realization and Approximation Problems*. Hoboken, NJ, USA: Wiley, 1957.
- [31] A. Ascoli, P. Curran, and O. Feely, "Modelling the dynamics of log-domain circuits," *Int. J. Circuit Theory Appl.*, vol. 35, no. 1, pp. 33–70, 2007.
- [32] F. Corinto, A. Ascoli, and M. Gilli, "Nonlinear dynamics of memristor oscillators," *IEEE Trans. Circuits Syst. I, Reg. Papers*, vol. 58, no. 6, pp. 1323–1336, Jun. 2011.
- [33] A. Ascoli et al., "A deep study of resistance switching phenomena in TaO_x ReRAM cells: System-theoretic dynamic route map analysis and experimental verification," *Adv. Electron. Mater.*, vol. 8, no. 8, 2022, Art. no. 2200182, doi: [10.1002aelm.202200182](https://doi.org/10.1002aelm.202200182).
- [34] F. Corinto, M. Forti, and L. O. Chua, *Nonlinear Circuits and Systems With Memristors—Analogue Computing via the Flux-Charge Analysis Method*. Cham, Switzerland: Springer, 2020.



Alon Ascoli (Senior Member, IEEE) received the Master of Science degree (Hons.) in electronic engineering from Universita' degli Studi Roma Tre in 2001, the Ph.D. degree in electronic engineering from University College Dublin in 2006, and the German Habilitation degree (Full Professor) in nonlinear circuit theory in 2022. He has been affiliated with Technische Universität Dresden since 2012, where he holds a lifelong position as a researcher and a lecturer since 2018. He develops theoretical concepts enabling to harness disruptive nanotechnologies to overcome traditional circuits' limitations for applications of interest to the more-than-Moore electronics era. In 2017, he was conferred the habilitation title as an Associate Professor in electrical circuit theory from the Italian Ministry of Education. He was a Visiting Research Scholar at the University of California Santa Cruz in 2019. Since October 2020, he has been a member of the IEEE Nanoelectronics and Gigascale Systems Technical Committee (Nano-Giga TC). In 2007, he was honored with the *International Journal of Circuit Theory and Applications (IJCTA)* Best Paper Award for the manuscript Modeling the dynamics of log-domain circuits. In September 2020, he was conferred the Best Paper Award on Electronics at the International Conference on Modern Circuits and Systems Technologies (MOCAST). He is the President of the IEEE Circuits and Systems (CAS) Cellular Nanoscale Networks and Memristor Array Computing (CNN-MAC) Technical Committee (TC) since 2021. He served as the President of the IEEE CAS Cellular Nanoscale Networks and Array Computing (CNNAC) TC from 2019 to 2021. He was the Chair of the 7th Memristor and Memristive Symposium, held in Catania (Italy), in 2021. He is the Guest Co-Editor for the Special Issue on Memristive Circuits and Systems for Edge-Computing Applications, to appear in December 2022 on the IEEE CAS JOURNAL ON EMERGING AND SELECTED TOPICS IN CIRCUITS AND SYSTEMS (JETCAS). He served as the Co-Chair of the IEEE Circuits and Systems Society (CASS) Seasonal School on Intelligence in Chips: Integrated Sensors and Memristive Computing, held online, over the time span November 2022.

nanotechnologies to overcome traditional circuits' limitations for applications of interest to the more-than-Moore electronics era. In 2017, he was conferred the habilitation title as an Associate Professor in electrical circuit theory from the Italian Ministry of Education. He was a Visiting Research Scholar at the University of California Santa Cruz in 2019. Since October 2020, he has been a member of the IEEE Nanoelectronics and Gigascale Systems Technical Committee (Nano-Giga TC). In 2007, he was honored with the *International Journal of Circuit Theory and Applications (IJCTA)* Best Paper Award for the manuscript Modeling the dynamics of log-domain circuits. In September 2020, he was conferred the Best Paper Award on Electronics at the International Conference on Modern Circuits and Systems Technologies (MOCAST). He is the President of the IEEE Circuits and Systems (CAS) Cellular Nanoscale Networks and Memristor Array Computing (CNN-MAC) Technical Committee (TC) since 2021. He served as the President of the IEEE CAS Cellular Nanoscale Networks and Array Computing (CNNAC) TC from 2019 to 2021. He was the Chair of the 7th Memristor and Memristive Symposium, held in Catania (Italy), in 2021. He is the Guest Co-Editor for the Special Issue on Memristive Circuits and Systems for Edge-Computing Applications, to appear in December 2022 on the IEEE CAS JOURNAL ON EMERGING AND SELECTED TOPICS IN CIRCUITS AND SYSTEMS (JETCAS). He served as the Co-Chair of the IEEE Circuits and Systems Society (CASS) Seasonal School on Intelligence in Chips: Integrated Sensors and Memristive Computing, held online, over the time span November 2022.



Ahmet S. Demirkol received the Ph.D. degree in electronics engineering from Istanbul Technical University, in 2014. From 2015 to 2019, he was a Lead Researcher in a joint industrial project at the Chair of Fundamentals of Electrical Engineering. Since 2019, he has been a Research Associate with the Chair of Fundamentals of Electrical Engineering, Technische Universität Dresden (TU Dresden). His current research interests cover modeling of memristors, analysis and design of memristive systems, cellular nonlinear networks, and neuromorphic circuit design, while he has a strong research experience in distortion analysis of RF switches using Volterra series, compact device modeling, analog circuit design, active networks synthesis, nonlinear dynamics, and chaos.



Ronald Tetzlaff (Senior Member, IEEE) is currently the Chief Officer for Technology Transfer and Internationalization with Technische Universität Dresden, Dresden, Germany, where he also holds a Full Professorship in Fundamentals of Electrical Engineering. His scientific interests include problems in the theory of signals and systems, medical signal processing, stochastic processes, systems modeling, systems identification, machine learning, mem-elements, memristive systems, Volterra systems, and cellular nonlinear networks. He was a Distinguished Lecturer of the IEEE CAS Society, from 2001 to 2002. He is a member of CAS CNN-MAC TC, the IEEE CAS Nano-Giga TC, German Society of Electrical Engineers, and Informationstechnische Gesellschaft (ITG) im Verband der Elektrotechnik, Elektronik, Informationstechnik (VDE) eingetragener Verein (e.V.). He founded the Chua Memristor Center in 2016. He served as an Associate Editor for the IEEE TRANSACTIONS ON CIRCUITS AND SYSTEMS—I, REGULAR PAPERS from 1999–2003.



Leon O. Chua (Life Fellow, IEEE) is widely known for the invention of the Memristor. His research has been recognized through 16 honorary doctorates from major universities in Europe and Japan, and seven U.S. patents. He was elected a fellow of IEEE in 1974, a Foreign Member of the European Academy of Sciences (Academia Europaea) in 1997, a Foreign Member of the Hungarian Academy of Sciences in 2007, and a Honorary Fellow of the Institute of Advanced Study at the Technical University of Munich, Germany, in 2012.